Published in final edited form as:
*J Am Chem Soc*. 2008 December 31; 130(52): 17761–17773. doi:10.1021/ja805033j.

# Helical Lanthanide(III) Complexes with Chiral Nonaaza Macrocycle

**Janusz Gregoliński**[†], **Przemysław Starynowicz**[†], **KimNgan T. Hua**[‡], **Jamie L. Lunkley**[‡], **Gilles Muller**[†], and **Jerzy Lisowski**[†]

†*Department of Chemistry, University of Wrocław, 14 F. Joliot-Curie, 50-383 Wrocław, Poland. Fax: 48 71 3282348; Tel: 48 71 3757252*

‡*Department of Chemistry, San José State University, One Washington Square, San José, CA 95192-0101, USA. Fax: 408-924-4945, Tel: 408-924-4973*

## Abstract

The chiral nonaazamacrocyclic amine **L**, which is a reduction product of the 3+3 Schiff base macrocycle, wraps around the lanthanide(III) ions to form enantiopure helical complexes. These Ce (III), Pr(III), Nd(III), Eu(III), Gd(III), Tb(III), Er(III), Yb(III) and Lu(III) complexes have been isolated in enantiopure form and have been characterized by spectroscopic methods. X-ray crystal structures of the Ln(III) complexes with **L** show that the thermodynamic product of the complexation of the *RRRRRR*-isomer of the macrocycle is the (*M*)-helical complex in the case of Ce(III), Pr(III), Nd(III) and Eu(III). In contrast, the (*P*)-helical complex is the thermodynamic product in the case of Yb(III) and Lu(III). The NMR and CD spectra show that the (*M*)-helicity for the kinetic complexation product of the *RRRRRR*-isomer of the macrocycle is preferred for all investigated lanthanide(III) ions, while the preferred helicity of the thermodynamic product is (*M*) for the early lanthanide(III) ions and (*P*) for the late lanthanide(III) ions. In the case of the late lanthanide(III) ions, a slow inversion of helicity between the kinetic (*M*)-helical product and the thermodynamic (*P*)-helical product is observed in solution. For Er(III), Yb(III) and Lu(III) both forms have been isolated in pure form and characterized by NMR and CD. The analysis of 2D NMR spectra of the Lu(III) complex reveals the NOE correlations that prove that the helical structure is retained in solution. The NMR spectra also reveal large isotopic effect on the $^1$H NMR shifts of paramagnetic Ln(III) complexes, related to NH/ND exchange. Photophysical measurements show that $\mathbf{L}_{RRRRRR}$ appears to favour an efficient $^3\pi\pi^*$-to-Ln energy transfer process taking place for Eu(III) and Tb(III), but these Eu(III)- and Tb(III)-containing complexes with $\mathbf{L}_{RRRRRR}$ lead to small luminescent quantum yields due to an incomplete intersystem crossing (isc) transfer, a weak efficiency of the luminescence sensitization by the ligand, and/or efficient non-radiative deactivation processes. Circularly polarized luminescence on the MeOH solutions of Eu(III) and Tb(III) complexes confirms the presence of stable chiral emitting species and the observation of almost perfect mirror-image CPL spectra for these compounds with both enantiomeric forms of **L**.

## Introduction

Both macrocyclic and helical structures continue to attract a lot of attention in inorganic and supramolecular chemistry. In some cases both structural motifs are combined[1–6], e.g. when binding of metal ion forces a large macrocycle to adopt a twisted conformation[2–4]. In such a conformation the two halves of the macrocycle form a double helical system. Controlling the helicity at higher organizational order e.g. that of metal complex, supramolecular assembly, polymer or liquid crystal, is an important but difficult task.[7] The chirality of metal complexes and inorganic supramolecular systems may be related e.g. to the spatial disposition of chelating

Correspondence to: Gilles Muller, gilles.muller@sjsu.edu; Jerzy Lisowski, jurekl@wchuwr.chem.uni.wroc.pl.

ligands around the metal ion,[7a] formation of single, double or triple helices,[8] helical twist of macrocyclic ligand,[2–5] or rotation of the side arms of the macrocycle[9]. The chiralilty at higher hierarchical order may sometimes be controlled by the chirality of the molecular building blocks (e.g. ligands in inorganic systems, monomers in polymeric systems, dopants in liquid crystals or polymeric systems). Thus the enantiopure supramolecular assemblies and metal complexes can be obtained in diastereoselective synthesis by using non-racemic chiral ligands, which may determine the chirality of the supramolecular assembly or metal complex (e.g. the handedness of the helical structure). Generally, this strategy is successful when one of the possible diastereomers is thermodynamically favoured.[9,10] In rare cases two diastereomeric structures of opposite helicity can be obtained for the same chirality of the molecular building blocks. Interconversion of such diastereomers corresponds to a helix inversion process. Helix inversion[2,3a,11–15] between well-defined and well-characterized diastereomers is a very rare phenomenon and is related to the transformation of the normal right-handed B-DNA into the left-handed Z-DNA[16], induced by high salt concentrations. Helicity induction and inversion are attracting a lot of attention in many areas of chemistry as general phenomena, related to functioning of biological systems, enantioselective catalysis and chiral recognition.

In a recent communication we have reported a new example of helical complexes based on nonaaza macrocycle **L** (Scheme 1), which is a reduced derivative of a 3+3 condensation product of 2,6-diformylpyridine and trans-1,2-diaminocyclohexane.[2] This 3+3 macrocycle exhibits much higher helical twist in its Ln(III) complexes in comparison with the Ln(III) complexes of the related chiral 2+2 macrocycles[3], or 3+3 macrocycle[5] derived from 2,6-diformylphenol. The chiral ligand **L** can be obtained in enantiopure forms $\mathbf{L}_{RRRRRR}$ and $\mathbf{L}_{SSSSSS}$, corresponding to all-*R* or all-*S* configuration of the diaminocyclohexane carbon atoms, respectively.[17] We have also demonstrated helicity inversion between the kinetic and the thermodynamic complexation product in the Yb(III) complexes of **L**.

In this contribution we present the synthesis of new enantiopure Ln(III) complexes of **L**, as well as the influence of the size of Ln(III) ion on the relative stability of the (P)/(M) diastereomers and helicity inversion process (Scheme 2). We also present luminescence, circularly polarized luminescence (CPL) and NMR characterization of the complexes in solution and discuss the effect of NH/ND exchange on $^1$H NMR paramagnetic shifts.

## Results and Discussion

### Synthesis

The macrocycle **L**was synthesized previously in a direct 3+3 condensation of enantiopure trans-1,2-diaminocyclohexane and 2,6-diformylpyridine, followed by reduction of the obtained macrocyclic Shiff base.[17b] On the other hand, in a later report[17a] it was shown that in fact a mixture of macrocyclic products was formed in this 3+3 condensation, and that Cd (II) template was necessary for the isolation of the pure product. It should also be noted that the same condensation reaction run in the presence of Ln(III) template leads to 2+2 macrocycle.[3] We have synthesized the macrocyclic amine $\mathbf{L}_{RRRRRR}$ and its enantiomer $\mathbf{L}_{SSSSSS}$ in a modified procedure. While it turned out that the Cd(II) ions are not necessary in the synthesis of **L**, short reaction times, higher dilution and recrystallization of the product are crucial for the isolation of the pure macrocycyle. The identity of **L** was confirmed by the X-ray crystal structure of its hydrochloride derivative, identical to that previously[17a] reported.

The [Ln**L**]$(NO_3)_3$ complexes exhibit good solubility in water and polar organic solvents, and often they are difficult to crystallize and to give pure products. On the other hand, the derivatives such as (*M*)-[Eu$\mathbf{L}_{RRRRRR}$]$_2$[Eu$(NO_3)_5$]$(NO_3)_4$•2$H_2O$, containing the complex counter-anions of the type $[Ln(NO_3)_5]^{2-}$, exhibit lower solubility and higher tendency to crystallize.[2] While the solution NMR studies of complexation of Ln(III) ions by **L** showed

successful incorporation of the metal ion in the macrocycle in each case, the isolation of pure complexes presented some problems in the case of Tb(III) and Er(III) ions, which exhibit similar preference for the (*P*)- and (*M*)-diastereomeric forms of the ligand (vide infra). In the case of Er(III) and Lu(III), it was possible to obtain both diastereomeric complexes, i.e. (*M*)-[Ln$\mathbf{L}_{RRRRRR}$]$(NO_3)_3$ and (*P*)-[Ln$\mathbf{L}_{RRRRRR}$]$(NO_3)_3$ in enantiopure form. The isolation of the (*P*)-isomer was based on the longer reaction times and use of a 6.5% molar excess of the ligand **L** (method A) or use of the (*M*)-isomer as a substrate and extended heating time (method B). In the case of Eu(III) and Tb(III) complexes, the isolation of the pure (*P*)-[Ln$\mathbf{L}_{RRRRRR}$]$(NO_3)_3$ isomers was not possible, although method B together with fractional recrystallization allowed to obtain fractions of the complex mixtures enriched in isomer (P) (the molar ratio *(M)/(P)* equal to 1:1 and 1:0.8 for Eu(III) and Tb(III) complexes, respectively).

The identity of the complexes has been confirmed by elemental analyses and mass spectra. The positive-mode ESI-MS spectra (Supporting Fig. S1) of methanol solutions of the complexes show peaks at *m/e* corresponding to the presence of the cationic complexes $[Ln\mathbf{L}]^{3+}$, in addition to ions $\{[Ln\mathbf{L}](NO_3)\}^{2+}$ and $\{[Ln\mathbf{L}](NO_3)_2\}^{+}$ arising from the ion clusterisation (Supporting Figs. S1 and S2). Sometimes the peak of $[Ln\mathbf{L}_{-\mathbf{H}}]^{2+}$ can also be observed (Fig. S1). The (*M*)-[Ln$\mathbf{L}_{RRRRRR}$]$(NO_3)_3$] and (*P*)-[Ln$\mathbf{L}_{RRRRRR}$]$(NO_3)_3$] diastereomers give rise to practically the same ESI-MS spectra, thus confirming their isomeric nature and similar chemical character (Supporting Fig. S2).

## X-ray crystal structures – helical conformation of the $[LnL]^{3+}$ complexes in solid state

Since the cavity formed by the nine nitrogen atoms in the “open” conformation of **L** (observed in its protonated form[17a]) is far too large for a single metal ion, the macrocycle **L** has to wrap very tightly around the $Ln^{3+}$ ion in a helical fashion in order to form a nine-coordinate complex. As a result of this twist, the two symmetry related halves of the macrocycle form a double helix system as observed in crystals of (*M*)-[Pr$\mathbf{L}_{RRRRRR}$]$(NO_3)_3$•$3CH_3CN$•$3^2/_3H_2O$, (*P*)-[Ce$\mathbf{L}_{SSSSSS}$]$(NO_3)_3$•$4CH_3CN$•$3H_2O$ and (*P*)-[Lu$\mathbf{L}_{RRRRRR}$]$(NO_3)_3$•$1^7/_8CH_3CN$•$3^3/_4H_2O$ (Scheme 2, Fig. 1, Supporting Fig. S3).

Although the molecular structures of the (*P*)-[Ce$\mathbf{L}_{SSSSSS}$]$^{3+}$ and (*P*)-[Lu$\mathbf{L}_{RRRRRR}$]$^{3+}$ cationic complexes look similar at first sight (Fig. 1), they in fact belong to two types of complexes. The **Type I** of $[Ln\mathbf{L}]^{3+}$ complexes corresponds to the series of (*M*)-[Ln$\mathbf{L}_{RRRRRR}$]$^{3+}$ complexes and their antipodes (*P*)-[Ln$\mathbf{L}_{SSSSSS}$]$^{3+}$, while the **Type II** corresponds to the series of (*P*)-[Ln$\mathbf{L}_{RRRRRR}$]$^{3+}$ complexes and their antipodes (*M*)-[Ln$\mathbf{L}_{SSSSSS}$]$^{3+}$. Thus the (*M*)-[Pr$\mathbf{L}_{RRRRRR}$]$^{3+}$ and (*P*)-[Ce$\mathbf{L}_{SSSSSS}$]$^{3+}$ complex cations constitute a quasi-enantiomeric pair of complexes and the mirror image of the (*P*)-[Ce$\mathbf{L}_{SSSSSS}$]$^{3+}$ cation is very similar to the (*M*)-[Pr$\mathbf{L}_{RRRRRR}$]$^{3+}$ cation.

The main difference between the two types of $[Ln\mathbf{L}]^{3+}$ complex is the direction and extent of helical twist of the macrocycle. This twist is reflected by the angle formed by the C3-C38 and C18-C23 bonds (Supporting Fig. S3). For the **Type I** complexes and the $\mathbf{L}_{RRRRRR}$ enantiomer of the ligand one observes the C3-C38-C18-C23 angle values equal to −172.6° for the Ce(III) complex, −174.4° for the Pr(III) complex, −186.8° and −185.5° for the two independent Eu (III) complex molecules[2], respectively, and −192.5° and −193.8° for the two independent Yb (III) complex molecules[2], respectively. The increase of the values of the C3-C38-C18-C23 angle with the decreasing radius of the metal ion indicates a tighter wrapping of the macrocycle **L** around the Ln(III) ion. For the **Type II** complexes the extent of helical twist of the macrocycle is larger. Importantly, the direction of the C3-C38-C18-C23 angle is opposite to that observed for the **Type I** complexes. The value of this angle is equal to 254.8° and 255.6° for the (*P*)-[Lu$\mathbf{L}_{RRRRRR}$]$^{3+}$ and (*P*)-[Yb$\mathbf{L}_{RRRRRR}$]$^{3+}$ cationic complexes, respectively. The positive value reflects the opposite helical twist sense of the $\mathbf{L}_{RRRRRR}$ macrocycle in comparison with the **Type I** complexes. The **Type I** and **Type II** diastereomers differ also in the configuration[18]

at the amine nitrogen atoms. The three 2,6-substituted pyridine fragments of the macrocycle **L** in the $[Lu\mathbf{L}]^{3+}$ complexes form propeller-like structure (Supporting Figs. S4, S5), similar to that observed in tris(dipicolinato)lanthanide anions[19]

The helical conformation of the ligand was clearly observed also in model structures of three other complexes of $\mathbf{L}_{RRRRRR}$ (see Supporting Information). In total six X-ray crystal structures correspond to **Type I** complexes and three structures correspond to **Type II** complexes. Importantly all crystals of **Type I** complexes correspond to the lighter lanthanide(III) ions or complexes of heavier lanthanide(III) ions obtained using relatively short reaction times, while all the **Type II** structures correspond to crystal of complexes of the heavier Yb(III) and Lu(III) ions obtained using longer reaction times or crystals obtained from the **Type I** Yb(III) complex grown for an extended period of time. The discussed structures indicate the preferred (*M*)-helicity of the $\mathbf{L}_{RRRRRR}$ ligand in the complexes with the lighter lanthanide ions and (*P*)-helicity of the ligand in the thermodynamic complexation product with the heavier Ln(III) ions.

## Relative Stability of the (*M*)- and (*P*)- Diastereomers of the $[LnL]^{3+}$ Complexes and the Helicity Inversion Process

The crystalline **Type I** and **Type II** $[Ln\mathbf{L}](NO_3)_3$ complexes give rise to very distinct CD spectra, that are characteristic for each type. For example, the CD spectrum of (*M*)-$[Ce\mathbf{L}_{\mathbf{RRRRRR}}]^{3+}$ is similar to that of the structurally characterized (*M*)-$[Yb\mathbf{L}_{\mathbf{RRRRRR}}]^{3+}$ complex[2], and the CD spectrum of the (*P*)-$[Lu\mathbf{L}_{\mathbf{RRRRRR}}]^{3+}$ complex to that of the structurally characterized (*P*)-$[Yb\mathbf{L}_{\mathbf{RRRRRR}}]^{3+}$ complex[2]. As expected the CD spectra of enantiomers are mirror images (Fig. 2, Supporting Fig. S8). Thus for a given $Ln^{3+}$ ion both the two diastereomeric **Type I** and **Type II** complexes and the enantiomers within each pair of these diastereomeric complexes can be distinguished on the basis of their characteristic CD spectra (Fig. 2, Fig. 3, Supporting Figs. S8, S9). Although all four stereoisomers of $[Ln\mathbf{L}]^{3+}$ complexes exhibit different CD spectra, the spectra of (*P*)-$[Ln\mathbf{L}_{RRRRRR}]^{3+}$ complexes resemble somewhat to those of the (*P*)-$[Ln\mathbf{L}_{SSSSSS}]^{3+}$ diastereomers and are very different when compared to the spectrum of the parent diastereomers (*M*)-$[Ln\mathbf{L}_{RRRRRR}]^{3+}$ (as is true for the other pair of diastereomers). This is in accord with the fact that the overall shape of the (*P*)-$[Ln\mathbf{L}_{RRRRRR}]^{3+}$ complex is similar to that of the (*P*)-$[Ln\mathbf{L}_{SSSSSS}]^{3+}$ diastereomer (Fig. 1). The above observations reflect the stronger influence of P/M helicity of these complexes on the CD spectra (e.g. via exciton-coupling mechanism) than the influence of R/S configuration at the cyclohexane fragments. The crystalline **Type I** and **Type II** $[Ln\mathbf{L}](NO_3)_3$ complexes give rise also to distinct $^1H$ NMR spectra, particularly for paramagnetic lanthanide(III) complexes (see NMR section below). The different CD and NMR spectra allow easy identification of the two types of complexes, as well as monitoring of the conversion of the one type of complex to the other type in solution.

The $[Ln\mathbf{L}]^{3+}$ complexes are relatively stable in solution at room temperature, as indicated by their NMR spectra (Fig. S10). However, the prolonged heating of the complexes in water solution results in partial ligand release (Fig. 4, Supporting Fig. S11 and Supporting Table S3). Generally, the (*M*)-$[Ln\mathbf{L}_{\mathbf{RRRRRR}}]^{3+}$ isomers are more stable for the early and middle lanthanide (III) ions with the exception of the Ce(III) complex, which decomposes completely after heating for 87 h at 318 K. This latter observation indicates that the slow ligand release is caused by the hydrolysis of the dissociated Ln(III) ions in water solution. The irreversible hydrolysis of the free Ln(III) ions into hydroxides in water solution at elevated temperature results in a shift of the complex dissociation equilibrium. In the case of Ce(III), the hydroxide is irreversibly oxidized to Ce(IV) dioxide (observed in the long-standing samples) what further shifts the dissociation equilibrium. The (*P*)-$[Ln\mathbf{L}_{\mathbf{RRRRRR}}]^{3+}$ diastereomers are more stable than the corresponding (*M*)-$[Ln\mathbf{L}_{\mathbf{RRRRRR}}]^{3+}$ diastereomers. For instance, the $D_2O$ solutions of (*P*)-$[YbL_{RRRRRR}]^{3+}$ show no decomposition to the ligand after addition of three equivalents of

HCl or NaOH (Fig. S12), while the (*M*)-[Ln$\mathbf{L}_{RRRRRR}$]$^{3+}$ diastereomers are quickly decomposed to Ln(III) hydroxides after addition of NaOH.

The NMR and CD spectra indicate that the (*M*)-[Ln$\mathbf{L}_{RRRRRR}$]$(NO_3)_3$ isomers convert to the (*P*)-[Ln$\mathbf{L}_{RRRRRR}$]$(NO_3)_3$ isomers in solution. The conversion of (*M*)-diastereomers into (*P*)-diastereomers corresponds to helicity inversion and is strongly dependent on the size of the Ln (III) ion. The helicity inversion of [Ln**L**]$^{3+}$ complexes is a slow process, taking weeks at room temperature. This process was followed in more details by recording the $^1$H NMR spectra of the $D_2O$ solutions of the complexes heated at 318 K over a period of two months. At this temperature the apparent first-order rate constant have been estimated to be in the order of $10^{-6}$ s$^{-1}$ (see Supporting Information). In the case of the smallest Ln(III) (Ln = Lu) ion, the (*P*)-isomeric form of the $\mathbf{L}_{RRRRRR}$ ligand is thermodynamically preferred and the conversion of the (*M*)-isomer, which is a kinetic product of complexation, is practically complete after heating for two weeks at 318 K (Fig. 4, Supporting Table S3). The (*P*)-isomer is also clearly thermodynamically preferred for the Yb(III) and Er(III) complexes (Supporting Fig. S11), while the Tb(III) exhibits comparable preference for the two diastereomeric forms (Fig. 4). In the case of Eu(III) complexes, the kinetic (*M*)-[Ln$\mathbf{L}_{RRRRRR}$]$^{3+}$ product is also a thermodynamic product, with the equilibrium ratio of the concentrations of the (*M*)- and (*P*)-diastereomers equal to 5:1 (Fig. 4). Finally, only the (*M*)-form is practically observed for the larger Ln(III) ions (Ln = Ce and Pr, Supporting Fig. S11).

The observed variation for the preferred helix direction along the series of lanthanide(III) ions reflects true thermodynamic effect, i.e. different equilibrium constants for the (*M*)-[Ln$\mathbf{L}_{RRRRRR}$]$^{3+}$ ↔ (*P*)-[Ln$\mathbf{L}_{RRRRRR}$]$^{3+}$ reaction, rather than the incomplete conversion process. This is proved by the behavior of the fractions of the Eu(III) complex mixtures enriched in isomer (*P*) (Supporting Figs. S13 and S14) with the (*M*)/(*P*) ratio ranging from 1:1 to 2:1. These fractions were enriched in the less soluble (*P*)-isomer in the process of fractional recrystallization and do not correspond to the equilibrium concentrations. However, when these samples are kept in solution for 20 days at room temperature, the equilibrium ratio of (*M*)/(*P*) equal to 5:1 is restored (Supporting Fig. S14). This experiment indicates that the observed helicity inversion process in the [Ln**L**]$^{3+}$ complexes is reversible.

## NMR spectroscopy – helical conformation of the [LnL]$^{3+}$ complexes in solution and unusual isotope effect on $^1$H NMR shifts

The $^1$H NMR spectra of the isolated Ce(III), Pr(III), Nd(III), Eu(III), Tb(III), Er(III), Yb(III) and Lu(III) complexes correspond to the presence of 29 signals, out of which 3 signals of exchangeable protons gradually disappear in solvents such as $D_2O$ or $CD_3OD$ (Supporting Figs. S12, S15–S20). This number of lines indicates that the complexed macrocycle **L** adopts a conformation of $C_2$ symmetry, in contrast to $D_3$ symmetry of the free ligand (reflected in the observation of 10 $^1$H NMR signals[17a]). In the case of the compounds with paramagnetic Ln (III) ions, the signals span a wide range, and the spectra of the two diastereomers, (*M*)-[Ln$\mathbf{L}_{RRRRRR}$]$(NO_3)_3$ and (*P*)-[Ln$\mathbf{L}_{RRRRRR}$]$(NO_3)_3$, are very different (Supporting Figs. S12, S18–S20). This reflects the high sensitivity of $^1$H NMR shifts of paramagnetic macrocyclic complexes to changes in complex structure.[3,20] On the other hand, the difference between the spectra of the two diastereomers of the Lu(III) complex is small (Supporting Fig. S21).

In the case of (*P*)-[Lu$\mathbf{L}_{RRRRRR}$]$(NO_3)_3$ and (*M*)-[Pr$\mathbf{L}_{RRRRRR}$]$(NO_3)_3$ complexes, it was possible to assign all the 29 signals on the basis of 2D NMR spectra (Fig. 5, Supporting Figs. S22–S25, see Supporting Information for details).

Apart from the crosspeaks, which are expected for the neighboring protons positioned close in space in ligand **L**, the ROESY spectra of the (*P*)-[Lu$\mathbf{L}_{RRRRRR}$]$(NO_3)_3$ complex exhibit additional crosspeaks corresponding to pairs of signals of protons **tn**, **tNH'**, **pNH'"**, **ug**,

**dNH”**, **nNH’”**, **un**, and **uNH’** (Fig. 5, see Scheme 1 for the labeling of the positions). In Scheme 1 these pairs do not correspond to protons that are close to each other. For the pairs **ug**, **nNH’”**, **tn** and **tNH’** the inter-proton distances in the X-ray crystal structure[7a] of the hydrochloride derivative of **L** are longer than 4–5 Å, hence the crosspeaks corresponding to these pairs are not expected for the “open” conformation of the macrocycle present in its free protonated form (Fig. 6). Since in the “open” conformation these distances are too long to explain the observation of clear NOE-type correlations in the ROESY spectra, the observation of additional “long range” ROESY correlations firmly indicates that the macrocycle **L** is considerably squeezed in its Ln(III) complexes. On the other hand, the analysis of the X-ray crystal structure of the (*P*)-[Lu$\mathbf{L}_{RRRRRR}$]$(NO_3)_3$ complex shows that the distances between the protons corresponding to the pairs of signals **tn, tNH’, pNH’”, ug, dNH”, nNH’”, un, and uNH’** are equal to 3.48, 3.60, 2.59, 2.60, 2.60, 2.14, 2.33 and 2.09 Å, respectively, and are fully consistent with the observation of the above NOE-type correlations (Fig. 6). As a result, the observation of the discussed additional ROESY crosspeaks proves that the helical conformation of the ligand, observed in the solid state, is retained in solution. The helical twist of the macrocycle is large enough to place closely in space protons that are positioned across the macrocycle in the “open” conformation. In other words, the two protons in each pair giving rise to additional ROESY correlations (**tn**, **tNH’**, **pNH’”**, **ug**, **dNH”**, **nNH’”**, **un**, and **uNH’**) belong to the two symmetry related halves of the macrocycle (Fig. 6).

In addition to P/M helicity inversion process, which takes weeks at room temperature, another faster process is revealed by the $^1$H NMR spectra. The $^1$H NMR spectra of the $D_2O$, $CD_3OD$, or $CD_3OD/CDCl_3$ solutions of the (*M*)-[Ln$\mathbf{L}_{RRRRRR}$]$(NO_3)_3$ complexes with the paramagnetic lanthanide(III) ions exhibit rather unexpected behavior in time. For the freshly prepared solutions 29 signals are observed, as discussed above. With time a new set of lines gradually appears. The new lines are very close to the original signals, so apparent doubling of signals is observed (Fig. 7–Fig. 9, Supporting Figs. 20, 26). This doubling effect is most pronounced for the strongly paramagnetically shifted resonances, except the signals of the NH protons, which gradually disappear at the same time. Finally, all of the original resonances within each doublet gradually disappear, and a set of 26 lines remains. This unexpected effect is explained by the integration of signals. The changes in time of the relative intensity of the original signals and their gradually growing twin counterparts follow the trend of the disappearance of the amine NH signals (Fig. 7, Fig. 9, Supporting Fig. S26). This proves, that apparent doubling of the resonances is related to the NH/ND exchange (Scheme 3), i.e. the original set of lines corresponds to the complex isotopologue with non-deuterated amine, while the final set of lines corresponds to the complex isotopologue with deuterated amine positions.

This explanation is additionally supported by the fact that the largest shift differences between the original signal and the new signal are observed for the positions close to the amine nitrogen atoms, e.g. protons **o**, **t**, **e** and **u** (Fig. 7, Fig. 8). The observed apparent splitting of signals represent an interesting case of isotope effect, since the influence of deuteration of the nitrogen atoms on the $^1$H NMR shifts of the adjacent carbon-attached protons is very strong. The maximum differences between the shift values of the non-deuterated and deuterated isotopologues, $\Delta^1$H(D), amount to 460, 320, 190 and 280 ppb for the Yb(III), Tb(III), Eu(III) and Pr(III) **Type I** complexes, respectively.

The discussed isotope effect is even larger for the **Type II** complex (*P*)-[Yb$\mathbf{L}_{RRRRRR}$]$(NO_3)_3$•$6H_2O$, with the maximum $\Delta^1$H(D) value as high as 500 ppb (Fig. 9). The NH/ND exchange process is much faster than the P ↔ M helicity inversion process, as seen in Suppporting Fig. S26. For example, the apparent first-order rates for this exchange ($CD_3OD$ solutions, 298K) are equal to $1.54\times10^{-4}$ s$^{-1}$ and $1.65\times10^{-4}$ s$^{-1}$ for the two different NH positions of the (*P*)-[Yb$\mathbf{L}_{RRRRRR}$]$(NO_3)_3$•$6H_2O$ complex, $1.15\times10^{-4}$ s$^{-1}$ for the *(M)*-[Pr$\mathbf{L}_{RRRRRR}$]$(NO_3)_3$•$H_2O$ complex and $1.0\times10^{-4}$ s$^{-1}$ for the (*M*)-[Yb$\mathbf{L}_{RRRRRR}$]$(NO_3)_3$]

•$CHCl_3$•$H_2O$ complex (Figs. S33, S34). The deuteration of amine nitrogen atoms in the $[Ln\mathbf{L}]^{3+}$ complexes is accelerated by bases such as triethylamine (Fig. 9, Supporting Fig. S27) and is inhibited by acids such as $HNO_3$ (Supporting Fig. S27). This influence of acid/base on the NH/ND exchange is opposite to that expected for associative mechanism of deuteration of free amine ligand **L**, i.e. protonation of amine nitrogen atoms. The observed effects may be explained for instance by dissociative mechanism of deuteration of complexed amine (i.e. deprotonation of NH groups), with the amide type $[Ln\mathbf{L}_{-\mathbf{H}}]^{2+}$ complexes as intermediates. As mentioned above, the $[Ln\mathbf{L}_{-\mathbf{H}}]^{2+}$ species were observed in the ESI-MS spectra. The somewhat different rates of NH/ND exchange for the non-equivalent nitrogen positions in the same complex indicate that the deuteration process corresponds to intact complex and is not related to dissociation of the ligand.

Large isotope effects on the $^1$H NMR shifts were previously observed for some metalloproteins containing iron porphyrins[21] and synthetic iron porphyrins[22]. In both cases, the magnitude of the shift difference is predominantly determined by the presence of paramagnetic metal ion, and the isotope effect arises from the change of the contact contribution to the isotropic shift. Large isotope effects on $^1$H NMR shifts are also observed in hydrogen-bonded systems.[23] In our case, the observed unusually large isotope effect may reflect the sensitivity of dipolar shifts to subtle changes in the complex structure.

## Photophysical and chiroptical properties

The intense band observed in the electronic spectrum of $\mathbf{L}_{\boldsymbol{RRRRRR}}$ at 37 585 $cm^{-1}$ is only slightly red-shifted upon complexation with Ln(III) ions (ca. 815 $cm^{-1}$, Table 1). On the other hand, ligand emission is observed for the complexes. Fluorescence from a short-lived $^1\pi\pi^*$ state occurs for all complexes while ligand phosphorescence from a long-lived $^3\pi\pi^*$ state is seen for the Gd(III) complex only, an efficient $^3\pi\pi^*$-to-Ln energy transfer process taking place for Eu(III) and Tb(III) and resulting in metal-centred emission exclusively (Supporting Fig. S28). The emission from the ligand $^1\pi\pi^*$ state in the Eu(III) and Tb(III) complexes suggests an incomplete intersystem crossing (isc) from the singlet to the triplet state.

The very small fluorescence quantum yields of the free ligand ($Q^F$ = 0.8%) and complexed ligand in the Gd(III) complex ($Q^F$ = 0.7%) confirmed that $\mathbf{L}_{\boldsymbol{RRRRRR}}$ is weakly luminescent. The quantum yields of the metal-centred luminescence obtained upon ligand excitation are small, $Q^{Ln}{}_L$ = 0.03 and 3.0% for Eu and Tb, respectively. They may be explained by the weak efficiency of the isc process, the emission from the $^1\pi\pi^*$ is still visible on the emission spectra, and by the relative energies of the triplet state of the complexed ligand and of the excited $^5D_0$ and $^5D_4$ levels (Fig. 10 and S28).[24] Another factor that may also largely contribute to the small quantum yields of the Eu(III) and Tb(III) complexes is the weak efficiency of the luminescence sensitization by the ligand ($\eta_{sens} = 7 \times 10^{-3}$, see Supporting Information). However, the presence of efficient non-radiative processes originated from the NH oscillators of the macrocyclic amine has a profound effect on the luminescence quantum yields. This effect is reflected in steady increase of luminescence intensity of the solutions of the (*M*)-$[Eu\mathbf{L}_{RRRRRR}](NO_3)_3$•$4H_2O$ complex in $CD_3OD$ (Fig. S30). The time-scale of this increase corresponds to slow deuteration of the amine nitrogen atoms observed in the NMR spectra discussed above (Scheme 3). The effect of NH oscillators has also been confirmed by the measurement of the luminescence lifetimes of the Eu(III) complex with $\mathbf{L}_{\boldsymbol{RRRRRR}}$ in MeOH and $CD_3OD$ ($\tau_{MeOH}$ = 0.18 ms and $\tau_{CD3OD}$ = 0.90 ms). Insertion to these τ values to the modified equation[25,26]:

$$\tau^{-1}_{CH_3OH} - \tau^{-1}_{CD_3OD} = q(1/A) + a + n_{NH}\gamma$$

(where $q$ is the number of coordinated water molecules, 1/A is a decay constant for the water molecule oscillators, γ is a decay constant for the amine NH oscillators, $n_{NH}$ is the number of NH groups and α is a correction for quenching by outer-sphere solvent molecules) gives negative q value of coordinated water molecules for the α, γ and A parameters taken from ref. 25 or 26. Since the NMR data for the Lu(III) complex indicate that the structure of the complex in solution corresponds to that in the solid state, most likely the structure of the (*M*)-[Eu$\mathbf{L}_{RRRRRR}$]$^{3+}$ cation in solution is also reflected by its X-ray crystal structure and water molecules are not bound to $Eu^{3+}$ ion. Substitution of q = 0, $n_{NH}$ = 6 and α = 0 in the above equation yields γ value equal to 0.74 $ms^{-1}$, which is smaller to that reported in ref. 25 (1.2 $ms^{-1}$) and ref. 26 (0.99 $ms^{-1}$). On the other hand, this γ value is similar to that of 0.759 $ms^{-1}$ determined[30] for NH oscillators in Eu(III) complexes of ethylenediamine. It should be noted that the number of studied cases is rather limited, and the differences in γ values may reflect the sensitivity of the quenching rate to the distance, as well as the influence of the possible H-bonds on the NH oscillators. Similarly, the lifetimes determined for the (*M*)-[Tb$\mathbf{L}_{RRRRRR}$]$^{3+}$ complex ($\tau_{MeOH}$ = 0.28 ms and $\tau_{CD3OD}$ = 0.31 ms) allow to calculate the γ constant for Tb(III) equal to 0.058 $ms^{-1}$, in comparison to 0.073 $ms^{-1}$ determined[27] for the Tb(III) complexes of ethylenediamine.

We have resorted to circularly polarized luminescence (CPL) to study the chiroptical properties of the Eu(III)- and Tb(III)-containing compounds. Generally speaking, CPL spectroscopy is the emission analog to circular dichroism (CD) spectroscopy. CD allows one to detect the differential absorption of left and right circularly polarized light, while CPL measures the difference in the emission intensity of left circularly polarized light versus right circularly polarized light. CPL has primarily been focused on studies aimed at investigating the chiral structures and solution dynamics of luminescent lanthanide complexes.[10a, 28, 29] The CPL spectra of 1 × $10^{-2}$ M solutions of the Eu(III) and Tb(III) complexes with each optical isomer of **L**, $\mathbf{L}_{RRRRRR}$ and $\mathbf{L}_{SSSSSS}$, are plotted in Figure 11 in the spectral range of the $^5D_0 \rightarrow {}^7F_1$ and $^5D_4 \rightarrow {}^7F_5$ transitions, which are particularly well-suited for CPL measurements since they satisfy the magnetic-dipole selection rule, $\Delta J = 0, \pm 1$ (except $0 \leftrightarrow 0$), respectively. The CPL spectra of each of these complex solutions were measured following excitation at 283–284 nm in MeOH at 295 K. As shown in Fig. 11, the detection of a CPL signal confirmed the presence of stable chiral emitting species on the luminescence time scale, and almost perfect mirror-image CPL spectra for the Eu(III) and Tb(III) complexes with both enantiomers, $\mathbf{L}_{RRRRRR}$ and $\mathbf{L}_{SSSSSS}$, were obtained. It is common to report the degree of CPL in terms of the luminescence dissymmetry factor, $g_{lum}(\lambda)$, which is defined as follows:

$$g_{lum} = \frac{\Delta I}{\frac{1}{2} I} = \frac{I_L - I_R}{\frac{1}{2}(I_L + I_R)}$$

where $I_L$ and $I_R$ refer, respectively, to the intensity of left and right circularly polarized emissions. The $g_{lum}$ values of the (*M*)-[Ln$\mathbf{L}_{RRRRRR}$]$^{3+}$ or (*P*)-[Ln$\mathbf{L}_{SSSSSS}$]$^{3+}$ (Ln = Eu and Tb) complexes amounted to +0.02 or −0.02 at 16 890 $cm^{-1}$, and −0.01, +0.06, and −0.02 or +0.01, −0.06, and +0.02 at 18 495, 18 445, and 18 210 $cm^{-1}$ in the spectral region of the $^5D_0 \rightarrow {}^7F_1$ (Eu) and $^5D4 \rightarrow {}^7F_5$ (Tb), respectively. These CPL results suggest that the emitted light is polarized in a direction determined by the helicity of the Eu(III) and Tb(III) ions, which in turn is controlled by the absolute configuration at the diaminocyclohexane carbon centers.

Although it was not possible to isolate the pure (*P*)- and (*M*)-diastereisomeric forms of the same Eu(III) or Tb(III) complex (i.e. [Ln$\mathbf{L}_{RRRRRR}$]$^{3+}$ or [Ln$\mathbf{L}_{SSSSSS}$]$^{3+}$), we have recorded the CPL spectrum of a 1 × $10^{-2}$ M solution containing a mixture of the (*M*)-[Eu$\mathbf{L}_{RRRRRR}$]$^{3+}$ and (*P*)-[Eu$\mathbf{L}_{RRRRRR}$]$^{3+}$ isomers with a (*M*):(*P*) ratio of 3.5:1 in MeOH. By comparing it to the one of (*M*)-[Eu$\mathbf{L}_{RRRRRR}$]$^{3+}$ (see Fig. 11), the observed CPL spectrum of the 3.5:1 (*M*)-

[Eu$\mathbf{L}_{RRRRRR}$]$^{3+}$:(*P*)-[Eu$\mathbf{L}_{RRRRRR}$]$^{3+}$ complex solution reveals several peaks corresponding to the contribution of each diastereoisomer present in solution. The CPL of the 3.5:1 (*M*)-[Eu$\mathbf{L}_{RRRRRR}$]$^{3+}$:(*P*)-[Eu$\mathbf{L}_{RRRRRR}$]$^{3+}$ complex solution shows that the weak single band, which is positive in sign, observed in the 16 665–16 835 cm$^{-1}$ region of the CPL of (*M*)-[Eu$\mathbf{L}_{RRRRRR}$]$^{3+}$ is made up of two components – positive and negative in sign – with the latter being the most intense. These results clearly indicate that the observed CPL changes (i.e. sign, magnitude and/or shape) are due to the influence of the different local helicity ((*M*) and (*P*)) at the metal center for the two diastereoisomers present in solution. Otherwise, mirror-image CPL spectra would be observed if the polarization of the emitted light would be controlled by the absolute configuration at the diaminocyclohexane carbon centers, as shown for (*M*)-[Ln$\mathbf{L}_{RRRRRR}$]$^{3+}$ and (*P*)-[Ln$\mathbf{L}_{SSSSSS}$]$^{3+}$ in Fig. 11. The observation of one peak centred at 16 875 cm$^{-1}$, and two peaks centred at 16 875 and 16 790 cm$^{-1}$ in the Eu(III) total luminescence spectra of (*M*)-[Eu$\mathbf{L}_{RRRRRR}$]$^{3+}$ (or (*P*)-[Eu$\mathbf{L}_{SSSSSS}$]$^{3+}$) and of the 3.5:1 (*M*)-[Eu$\mathbf{L}_{RRRRRR}$]$^{3+}$:(*P*)-[Eu$\mathbf{L}_{RRRRRR}$]$^{3+}$ complex solution is also consistent with the presence of each diastereoisomeric form of [Eu$\mathbf{L}_{RRRRRR}$]$^{3+}$ in the latter complex solution, respectively (Fig. 11). It should be noted that the observed CPL changes between the CPL spectra of a 1 × 10$^{-2}$ M (*M*)-[Tb$\mathbf{L}_{RRRRRR}$]$^{3+}$ complex solution measured before and after the solution was heated at 328 K for three weeks also confirmed that the polarization of the emitted light is controlled by the (*M*)/(*P*) helicity at the metal center. As shown in Fig. S29, noticeable spectral changes were observed in the Tb(III) total luminescence and CPL spectra. In agreement with the fact that Eu(III) in theory has a simpler crystal field energy level pattern than Tb(III), the spectral changes observed are less obvious for the Tb(III) systems than for the Eu(III) complex solutions.

## Conclusions

Both the X-ray crystal structures of the [Ln**L**](NO$_3$)$_3$ complexes and ROESY spectra of the Lu(III) complex show that the large nonaaza macrocycle **L** has to wrap thightly around the Ln (III) ions in order to form [Ln**L**]$^{3+}$ complexes. In these complexes the two halves of the ligand form a double-helical system. Moreover, the [Ln**L**](NO$_3$)$_3$ complexes can exist in two diasteromeric forms of opposite helicity, which have the same chirality at all stereogenic carbon centres and are synthesized from the same enantiomer of chiral ligand. For the all-*R* enantiomer of the ligand, the binding of the Ln(III) ions results in kinetic complexes of *M*-helicity, (*M*)-[Ln$\mathbf{L}_{RRRRRR}$]$^{3+}$. These *M*-helical complexes slowly convert in the helicity inversion process into the (*P*)-[Ln$\mathbf{L}_{RRRRRR}$]$^{3+}$ diastereomers. Unlike most known cases of helicity inversion[11–15], the described process corresponds to conversion between well-defined, exact diastereomers, which enantiopure forms have been characterized on the basis of NMR, CD, ESI-MS and X-ray crystal data. The helicity inversion process in [Ln**L**]$^{3+}$ complexes is strongly dependent on the size of Ln$^{3+}$ ion and is not observed for the lighter lanthanide(III) ions. Thus the (*M*)-[Ln$\mathbf{L}_{RRRRRR}$]$^{3+}$ complex is the theromodynamic product in the case of Pr(III) ion, while the (*P*)-[Ln$\mathbf{L}_{RRRRRR}$]$^{3+}$ complexes are the thermodynamic product in the case of Yb(III) and Lu(III) ions.

Finally, the CPL results (i.e. stable chiral emitting species and mirror image CPL spectra) are in line with the results of the CD and $^1$H NMR studies. As discussed above, the Ln(III) complexes are quite stable in solution at room temperature, while the conversion of (*M*)-diastereomer into (*P*)-diastereomer, corresponding to a helical inversion, is a slow process in methanol at room temperature (Supporting Fig. S10). On the other hand, the photophysical properties of the ligand **L** and its Ln(III) complexes demonstrate that the various energy conversion processes occurring in the former compounds are not optimum. In particular, an incomplete isc transfer, a weak efficiency of the luminescence sensitization by the ligand, and/or efficient non-radiative deactivation processes may largely contribute to the weak ligand- and metal-centered luminescent quantum yields.

## Experimental

### Measurements

The NMR spectra were taken on Bruker Avance 500 and AMX 300 spectrometers. The chemical shifts were referenced to the residual solvent signal or DSS. The gradient COSY, TOCSY, NOESY, ROESY and HMQC spectra were acquired using 512×1K data points and zero filled to 1K×1K matrix. Mixing times 25–200 ms were used in NOESY and ROESY experiments. The CD spectra were measured on Jasco J-715 Spectropolarimeter. The positive-mode electrospray mass spectra of ca. $1 \times 10^{-6}$ M methanol solutions of the complexes were obtained using Bruker microOTOF-Q instrument. The elemental analyses were carried out on a Perkin-Elmer 2400 CHN elemental analyzer. Electronic spectra in the UV/Vis range were recorded at 295 K with a Varian Cary 50Bio spectrometer using 1.0 and 0.1 cm quartz cells. Fluorescence and phosphorescence spectra were recorded on a Varian Cary Eclipse and Perkin-Elmer LS-50B spectrometers equipped for low temperature (77 K) measurements. Luminescence lifetimes were measured on the Varian Cary Eclipse utilizing the short phosphorescence decay software package. Quantum yields were determined using the following equation:

$$Q_x/Q_r=[A_r(\lambda_r)/A_x(\lambda_x)][I_r(\lambda_r)/I_x(\lambda_x)][n_x^2/n_r^2][D_x/D_r]$$

where $A$ is the absorbance at the excitation wavelength (λ), $I$ is the intensity of the excitation light at the same wavelength, $n$ is the refractive index, $D$ is the integrated luminescence intensity, and the subscript "$x$" refers to the sample and "$r$" to the reference. The spectra were corrected for instrumental functions. Quantum yields of the ligand- and metal-centred emissions were measured relative to quinine sulfate in 0.05 M $H_2SO_4$ ($Q^F$ = 54.6%)[30] and [Ln(2,6-pyridine-dicarboxylate = DPA)$_3$]$^{3-}$ in Tris buffer (0.1 M) for Eu ($Q^{Eu}_L$ = 13.5%)[30] and Tb ($Q^{Tb}_L$ = 26.5%)[31], respectively. CPL measurements were made on an instrument described previously, operating in a differential photon-counting mode.[28c,29b]

The crystallographic measurements were performed on κ–geometry Kuma KM4CCD automated four-circle diffractometers (ω–scan) with graphite–monochromatized Mo*K*α radiation. The data for the crystals were collected at 100(2) K. The data were corrected for Lorentz and polarization effects, and analytical absorption correction was applied. Data collection, cell refinement, and data reduction and analysis were carried out with the KM4CCD software (Oxford Diffraction Poland): CrysAlis CCD and CrysAlis RED, respectively.[32] The structures of complexes were solved by direct methods using the SHELXS-97 program.[33] The crystals of (*M*)-[Pr**L**$_{RRRRRR}$](NO$_3$)$_3$•3CH$_3$CN•3$^2/_3$H$_2$O, (*P*)-[Ce**L**$_{SSSSSS}$](NO$_3$)$_3$•4CH$_3$CN•3H$_2$O and (*P*)-[Lu**L**$_{RRRRRR}$](NO$_3$)$_3$•1$^7/_8$CH$_3$CN•3$^3/_4$H$_2$O were grown by slow evaporation of the methanol/acetonitrile solutions. Suitable crystals were cut from larger ones and mounted on a Kuma KM4 diffractometer. The structures were solved in a routine way (SHELXS97, SHELXL97)[33, 34], using the SHELXTL[35] program package. All figures were made with SHELXTL[35], MERCURY[36] and DIAMOND[37] programs. The structures suffered from partial disorder of solvent (water and acetonitrile) molecules. In (*P*)-[Lu**L**$_{RRRRRR}$](NO$_3$)$_3$•1$^7/_8$CH$_3$CN•3$^3/_4$H$_2$O 2.75 water and 0.875 acetonitrile molecules per asymmetric part were disordered. In (*M*)-[Pr**L**$_{RRRRRR}$](NO$_3$)$_3$•3CH$_3$CN•3$^2/_3$H$_2$O and (*P*)-[Ce**L**$_{SSSSSS}$](NO$_3$)$_3$•4CH$_3$CN•3H$_2$O all the water molecules were disordered and apart from that in (*P*)-[Ce**L**$_{SSSSSS}$](NO$_3$)$_3$•4CH$_3$CN•3H$_2$O a CH$_3$CN molecule was disordered, too. The positions of C- and N-bonded H atoms were calculated from geometry, excluding disordered acetonitrile molecules. All ordered non-H atoms were refined anisotropically, the disordered ones were isotropic and the isotropic thermal vibration factors of the H atoms were 1.2 times the trace of the anisotropic factors of relevant adjacent C or N atoms. The occupation factors of the disordered molecules were chosen so to warrant maximum filling of the space and were

not refined. The data pertinent to the data collection and refinement are given in Supporting Table S1.

## Synthesis

**$L_{RRRRRR}$ amine (or $L_{SSSSSS}$ amine)—**The solution of 1 mmol (135.1 mg) of 2,6-diformylpyridine in 43 ml of methanol was combined with the solution of 1 mmol (114.2 mg) of trans-(1*R*,2*R*)-diaminocyclohexane (or trans-(1*S*,2*S*)-diaminocyclohexane) in 7 ml of methanol and stirred for 30 min. at room temperature. The formed mixture of Schiff base macrocyles was reduced on a water bath with 12 mmol (454 mg) of $NaBH_4$, which was gradually added for 2 hrs. The stirring was continued for 2 hrs and the mixture was evaporated to dryness under reduced pressure. The residue was redissolved in 15 ml of water and solid NaOH was added until pH was ca. 14. The precipitated white solid was extracted with 3 × 5 ml of dichloromethane and the organic fractions were dried over anhydrous $Na_2SO_4$. The solution was filtered and evaporated to dryness. The crude product was purified by fractional recrystallization from dichloromethane/acetonitrile mixture. The obtained white product was filtered, washed with 1 ml of cold acetonitrile and dried. Yield 118.6 mg (54.58%). ESI-MS: m/z: 652.2 $C_{39}H_{58}N_9^+$; 674.2 $C_{39}H_{57}N_9Na^+$. $^1$H NMR ($CDCl_3$) δ 7.59 (3H, t); 7.21 (6H, d); 4.00 (6H, d); 3.78 (6H, d); 3.47 (6H, broad); 2.31 (6H, m); 2.03 (6H, m); 1.99 (6H, m); 1.01 - 1,24 (12H. m). Anal. Calc. (found) for $C_{39}H_{58}N_9O_{0.5}$: C, 70.87 (70.98); H, 8.84 (8.57); N, 19.07 (19.17).

**[LnL]$(NO_3)_3$•*n*$H_2O$ complexes of the Type I (Ln = Ce, Pr, Nd, Eu, Gd, Tb)—**The solution of 0.2 mmol (130.4 mg) of an appropriate enantiomer of macrocycle **L** in 8 ml of methanol was combined with the solution of 0.2 mmol of $Ln(NO_3)_3$•*n*$H_2O$ in 8 ml of methanol and the mixture was refluxed for 1 hr (30 min. in the case of Ce(III) complexes). The solution was evaporated to dryness and the residue was dissolved in a mixture of 2 ml of methanol and 8 ml of acetonitrile. The solution was concentrated on rotary evaporator until precipitate appeared. The mixture was left overnight in the freezer. The obtained precipitate was filtered, washed with small amounts of cold acetonitrile and dried.

**(*M*)-[Ce$L_{RRRRRR}$]$(NO_3)_3$•2$H_2O$—**Yield 137.3 mg (67.7%). ESI-MS: m/z: 263.8 $[CeL]^{3+}$, 426.7 $\{[CeL](NO_3)\}^+$, 915.5 $\{[CeL](NO_3)\}^{2+}$. $^1$H NMR (500 MHz, $D_2O$, 298K): δ −13.49, −8.64, −7.60, −1.81, −1.46, −1.46, −1.10, −0.73, −0.48, 0.29, 0.63, 1.13, 1.74, 1.93, 2.36, 2.43, 2.63, 2.83, 3.12, 3.12, 5.17, 6.38, 7.86, 8.29, 9.12, 9.23, 9.69, 10.04, 10.22. $^1$H NMR (500 MHz, $CD_3CN$, 298K): δ −15.35, −10.13, −8.40, −2.42, −1.75, −1.38, −1.00, −0.97, −0.64, 0.25, 0.50, 1.07, 2.17, 2.29, 2.40, 2.46, 2.70, 3.13, 3.15, 3.37, 5.60, 7.74, 7.93, 8.53, 9.15, 9.46, 9.73, 10.25, 10.33. Anal. calc. (found) for $CeC_{39}H_{61}N_{12}O_{11}$: C, 46.19 (46.14); H, 6.06 (5.74); N, 16.57 (16.70). CD [$H_2O$, 298K, $\lambda_{max}$/nm (ε/$M^{-1}cm^{-1}$)]: 192 (−26), 201 (−3.3), 210 (−7.1), 227 (0.7), 239 (−0.7), 264 (6), 279 (−1.8).

**(*P*)-[Ce$L_{SSSSSS}$]$(NO_3)_3$•2$H_2O$—**CD [$H_2O$, 298K, $\lambda_{max}$/nm (ε/$M^{-1}cm^{-1}$)]: 192 (25), 200 (3.7), 209 (7.6), 227 (−0.7), 240 (0.6), 264 (−6), 279 (1.8).

**(*M*)-[Pr$L_{RRRRRR}$]$(NO_3)_3$•$H_2O$—**Yield 141.2 mg (70.8%). ESI-MS: m/z: 264.1 $[PrL]^{3+}$, 427.2 $\{[PrL](NO_3)\}^+$, 916.4 $\{[PrL](NO_3)\}^{2+}$. $^1$H NMR (500 MHz, $D_2O$, 298K): δ −25.38, −21.16, −16.66, −15.54, −4.23, −3.92, −2.50, −1.96, −0.56, −0.56, −0.56, −0.05, −0.05, −0.05, 0.01, 0.08, 0.70, 1.29, 1.36, 1.80, 4.56, 5.95, 6.69, 7.47, 9.20, 12.60, 16.42, 21.27, 21.64. $^1$H NMR (500 MHz, $CD_3CN$, 298K): δ −28.05, −19.72, −17.41, −16.91, −4.46, −3.88, −2.70, −1.24, −0.52, −0.17, −0.15, −0.04, −0.03, 0.48, 1.27, 1.35, 1.69, 1.98, 3.6, 4.32, 6.41, 6.64, 7.92, 9.16, 12.48, 16.14, 20.90, 21.41. Anal. Calc. (found) for $PrC_{41}H_{72}N_{13}O_{15}$: C, 43.66 (43.60); H, 6.43 (6.13); N, 16.14 (16.21). CD [$H_2O$, 298K, $\lambda_{max}$/nm (ε/$M^{-1}cm^{-1}$)]: 192 (−25.3), 201 (−3.4), 209 (−6.2), 225 (1.1), 237 (−0.9), 267 (4.5) 280 (0.6), 284 (0.9).

**(*P*)-[PrL$_{SSSSSS}$](NO$_3$)$_3$•H$_2$O—**CD [H$_2$O, 298K, $\lambda_{max}$/nm ($\varepsilon$/M$^{-1}$cm$^{-1}$))]: 192 (24), 201 (3), 210 (6), 224 (−1), 238 (0.7), 266 (−4) 280 nm (−0.5), 284 (−1).

**(*M*)-[NdL$_{RRRRRR}$](NO$_3$)$_3$•0.5H$_2$O—**Yield of 150.7 mg (76.0%). ESI-MS: m/z: 396.2 [NdL$_{-H}$]$^{2+}$, 856.4 {[NdL$_{-H}$](NO$_3$)}$^+$, 919.3 {[NdL](NO$_3$)$_2$}$^+$. $^1$H NMR (500 MHz, D$_2$O, 298K): δ −17.21, −11.77, −3.81, −1.12, −0.58, −0.25, −0.13, 0.03, 0.12, 0.62, 0.86, 0.94, 1.93, 2.24, 2.57, 2.84, 3.43, 4.11, 4.59, 5.15, 5.57, 6.32, 6.96, 7.93, 7.93, 8.84, 9.59, 11.16, 17.35. $^1$H NMR (500 MHz, CD$_3$CN, 298K): δ −17.64, −11.40, −3.76, −0.88, −0.24, −0.24, −0.24, −0.08, 0.40, 0.70, 0.74, 0.90, 0.92, 2.12, 2.80, 3.21, 3.72, 3.90, 5.88, 6.71, 7.21, 8.10, 8.21, 8.63, 9.68, 11.08, 17.27. Anal. Calc. (found) for NdC$_{39}$H$_{58}$N$_{12}$O$_{10.5}$: C, 47.26 (47.20); H, 5.90 (5.68); N, 16.96 (16.92). CD [H$_2$O, 298K, $\lambda_{max}$/nm ($\varepsilon$/M$^{-1}$cm$^{-1}$)]: 192 (−22), 201 (−3.3), 210 (−6.6), 225 (0.4), 238 (−1.5), 264 (7), 279 (−1.2).

**(*P*)-[NdL$_{SSSSSS}$](NO$_3$)$_3$•0.5H$_2$O—**CD [H$_2$O, 298K, $\lambda_{max}$/nm ($\varepsilon$/M$^{-1}$cm$^{-1}$))]: 192 (22), 201 (3), 211 (−7), 225 (−0.5), 237 (1.0), 264 (−8), 279 (2.0).

**(*M*)-[EuL$_{RRRRRR}$](NO$_3$)$_3$•4H$_2$O—**Yield 160.8 mg (75.7%). NMR identical to that of the previously synthesized (*M*)-[Eu**L**$_{RRRRRR}$](NO$_3$)$_3$•CHCl$_3$•2H$_2$O complex[2]. Anal. Calc. (found) for EuC$_{39}$H$_{65}$N$_{12}$O$_{13}$: C, 44.11 (43.77); H, 6.17 (5.93); N, 15.83 (15.65). CD [H$_2$O, 298K, $\lambda_{max}$/nm ($\varepsilon$/M$^{-1}$cm$^{-1}$)]: 193 (−17), 200 (−5.8), 208 (−8.8), 228 (−0.5), 236 (−0.4), 263 (6), 278 (−0.9).

**(*P*)-[EuL$_{SSSSSS}$](NO$_3$)$_3$•4H$_2$O—**CD [H$_2$O, 298K, $\lambda_{max}$/nm ($\varepsilon$/M$^{-1}$cm$^{-1}$)]: 192 (−18), 201 (6.1), 208 (9.1), 227 (0.5), 236 (0.2), 264 (−5.4), 277 (−1.4).

**(*M*)-[GdL$_{RRRRRR}$](NO$_3$)$_3$•4H$_2$O—**Yield 136 mg (63.7%). ESI-MS: m/z: 269.8 [GdL]$^{3+}$, 404.2 [GdL$_{-H}$]$^{2+}$. Anal. Calc. (found) for GdC$_{39}$H$_{65}$N$_{12}$O$_{13}$: C, 43.89 (43.55); H, 6.14 (6.28); N, 15.75 (15.70). CD [H$_2$O, 298K, $\lambda_{max}$/nm ($\varepsilon$/M$^{-1}$cm$^{-1}$))]: 194 (−19), 201 (−8.2) 208 (−11), 224 (−1.3), 229 (−1.7), 263 (6.6), 278 (−0.8).

**(*M*)-[TbL$_{RRRRRR}$](NO$_3$)$_3$•4H$_2$O—**NMR identical to that of the previously synthesized (*M*)-[Tb**L**$_{RRRRRR}$](NO$_3$)$_3$•CHCl$_3$•2H$_2$O complex[2]. Anal. Calc. (found) for TbC$_{39}$H$_{65}$N$_{12}$O$_{13}$: C, 43.82 (43.51); H, 6.13 (5.81); N, 15.72 (15.53). CD [H$_2$O, 298K, $\lambda_{max}$/nm ($\varepsilon$/M$^{-1}$cm$^{-1}$)]: 193 (−19), 201 (−8.6), 207 (−8.7), 226 (−0.4), 230 (−0.8), 264 (3.7), 277 (−0.6).

**(*P*)-[TbL$_{SSSSSS}$](NO$_3$)$_3$•4H$_2$O—**CD [H$_2$O, 298K, $\lambda_{max}$/nm ($\varepsilon$/M$^{-1}$cm$^{-1}$)]: 193 (−20), 202 (7.6), 207 (7), 225 (0.1), 229 (0.3), 264 (−3.3), 278 (0.8).

**[LnL](NO$_3$)$_3$•CHCl$_3$•*n*H$_2$O complexes of the Type I (Ln = Er, Lu)—**The solution of 0.2 mmol (130.4 mg) of an appropriate enantiomer of macrocycle **L** in 8 ml of chloroform was combined with the solution of 0.2 mmol of Ln(NO$_3$)$_3$•*n*H$_2$O in 4 ml of methanol, and the mixture was refluxed for 40 min.. The mixture was filtered, the volume of the filtrate was reduced to ca. 6 ml and 8 ml of chloroform was added. The solution was concentrated on rotary evaporator until precipitate appeared and left overnight in the freezer. The obtained precipitate was filtered, washed with small amounts of cold chloroform and dried under vacuum.

**(*M*)-[ErL$_{RRRRRR}$](NO$_3$)$_3$•CHCl$_3$•2.5H$_2$O—**Yield 92.3 mg (39.5%). ESI-MS: m/z: 273.2 [ErL]$^{3+}$, 440.2 {[ErL](NO$_3$)}$^+$, 943.6 {[ErL](NO$_3$)}$^{2+}$. $^1$H NMR (500 MHz, D$_2$O, 298K): δ −41.41, −32.58, −10.95, −10.42, −8.99, −7.13, −6.27, −5.33, −2.76, −1.94, −1.17, −1.17, −0.46, −0.46, −0.46, 6.98, 6.98, 6.98, 8.07, 8.49, 14.29, 15.78, 15.78, 27.17, 37.08, 51.65, 68.96. Anal. Calc. (found) for ErC$_{40}$H$_{63}$N$_{12}$O$_{11.5}$Cl$_3$: C, 41.08 (40.87); H, 5.43 (5.25); N, 14.37 (14.68).

CD [$H_2O$, 298K, $\lambda_{max}$/nm ($\varepsilon/M^{-1}cm^{-1}$)]: 193 (−20), 206 (−8.4), 223 (−0.5), 231 (−1.0), 264 (3.9), 279 (−0.4).

**(*M*)-[LuL$_{RRRRRR}$](NO$_3$)$_3$•CHCl$_3$•2H$_2$O—**Yield 127.3 mg (54.5%). ESI-MS: m/z: 275.5 $[LuL]^{3+}$, 444.2 $\{[LuL](NO_3)\}^{+}$, 950.4 $\{[LuL](NO_3)\}^{2+}$. $^1$H NMR (500 MHz, $D_2O$, 298K): δ 0.78, 0.84, 0.96, 0.96, 1.16, 1.32, 1.41, 1.59, 1.62, 1.66, 1.77, 1.95, 2.15, 2.35, 2.55, 2.78, 3.30, 3.78, 3.98, 4.00, 4.22, 4.64, 4.52, 4.67, 7.48, 7.49, 7.57, 7.98, 8.04. Anal. Calc. (found) for: $LuC_{40}H_{62}N_{12}Cl_3O_{11}$ C, 41.12 (41.11); H, 5.35 (5.52); N, 14.39 (14.69). CD [$H_2O$, 298K, $\lambda_{max}$/nm ($\varepsilon/M^{-1}cm^{-1}$)]: 193 (−21), 223 (0.2),230 (−0.4), 264 (4.0) (−1).

### [LnL](NO$_3$)$_3$•*n*H$_2$O complexes of the Type II

**Method A (Ln =Lu). (*P*)-[LuL$_{RRRRRR}$](NO$_3$)$_3$•7H$_2$O—**The solution of 138.9 mg (0.213 mmol) of **L**$_{RRRRRR}$ in 5 ml of methanol was combined with 0.2 mmol (83 mg) of Lu $(NO_3)_3$•$3H_2O$ in 5 ml of methanol and the mixture was refluxed for 2 hrs. The solution was cooled down, 30 ml of acetonitrile was added in portions, the volume was reduced on a rotary evaporator until a precipitate appeared, and the mixture was left to stand in the freezer overnight. The obtained product was filtered, washed with cold acetonitrile and dried under vacuum. Yield 127.8 mg (57%). ESI-MS: m/z: 275.5 $[LuL]^{3+}$, 444.2 $\{[LuL](NO_3)\}^{+}$, 950.5 $\{[LuL](NO_3)\}^{2+}$. $^1$H NMR (500 MHz, $D_2O$, 298K): δ 0.78, 0.85, 1.02, 1.12, 1.19, 1.38, 1.54, 1.58, 1.67, 1.67, 1.67, 1.81, 2.14, 2.21, 2.26, 2.26, 3.09, 3.62, 3.71, 4.00, 4.16, 4.30, 4.60, 4.64, 7.48, 7.50, 7.60, 7.99, 8.04. $^{13}$C NMR (500 MHz, $D_2O$, 298K): δ 26.62, 26.92, 27.24, 33.07, 33.31, 33.73, 50.98, 53.88, 54.49, 62.09, 65.46, 67.57, 125.23, 126.03, 127.39, 144.48, 144.64, 159.43, 160.43, 163.16. Anal. Calc. (found) for $LuC_{39}H_{69}N_{12}O_{15}$: C, 41.99 (41.79); H, 6.20 (6.20); N, 15.19 (14.99). CD [$H_2O$, 298K, $\lambda_{max}$/nm ($\varepsilon/M^{-1}cm^{-1}$)]: 191 (51), 203 (16), 227 (−6.7), 271 (16).

**Method B (Ln = Er, Lu)—**0.1 mmol of an appropriate [Ln**L**](NO$_3$)$_3$•CHCl$_3$•*n*H$_2$O complex was dissolved in a mixture of 10 ml of acetonitrile and 4 ml of water. The solution was refluxed (120 hrs for Er(III) complex and 2 hrs for Lu complex), evaporated to dryness and redissolved in a mixture of 2 ml of methanol and 8 ml of acetonitrile. The solution was concentrated on rotary evaporator to ca. 5 ml, until precipitate appeared and was left overnight in the freezer. The obtained precipitate was filtered, washed with small amounts of cold acetonitrile and dried under vacuum.

**(*P*)-[ErL$_{RRRRRR}$](NO$_3$)$_3$•7H$_2$O—**Yield 43.1 mg (38.1%). ESI-MS: m/z: 273.2 $[ErL]^{3+}$, 440.8 $\{[ErL](NO_3)\}^{+}$, 943.8 $\{[ErL](NO_3)\}^{2+}$. $^1$H NMR (500 MHz, $D_2O$, 298K): δ −67.05, −18.89, −16.10, −16.10, −14.37, −12.12,−10.98, −8.75, −2 to 4.3 seven overlapped broad signals, 6.32, 6.87, 7.75, 9.94, 9.97, 10.20, 15.82, 23.36, 38.87, 72.43, 88.72, 157.10. Anal. Calc. (found) for $ErC_{39}H_{71}N_{12}O_{16}$: C, 41.41 (41.31); H, 6.33 (6.12); N, 14.86 (14.76). CD [$H_2O$, 298K, $\lambda_{max}$/nm ($\varepsilon/M^{-1}cm^{-1}$)]: 190 (49), 203 (18), 227 (−6.1), 272 (18).

**(*P*)-[LuL$_{RRRRRR}$](NO$_3$)$_3$•4.5H$_2$O—**Yield 67.3 mg (61.5%). Anal. Calc. (found) for $LuC_{39}H_{66}N_{12}O_{13.5}$: C, 42.82 (42.87); H, 6.08 (5.73); N, 15.36 (15.19).

The **(*M*)-[YbL$_{RRRRRR}$](NO$_3$)$_3$•CHCl$_3$•H$_2$O, (*M*)-[YbL$_{RRRRRR}$]$_2$[Yb(NO$_3$)$_5$](NO$_3$)$_4$•4H$_2$O, (*P*)-[YbL$_{RRRRRR}$](NO$_3$)$_3$•6H$_2$O** complexes have been obtained as described previously[2].

## Supplementary Material

Refer to Web version on PubMed Central for supplementary material.

## Acknowledgement

This work was supported by MNiSW grant 1 T09A 143 30. G.M. thanks the National Institutes of Health Minority Biomedical Research Support (2 S06 GM008192-24A1) and Research Corporation Cottrell Science Award (CC6624) for their financial support. We thank Prof. T. Lis for help with the determination of the X-ray crystal structures.

## References

1. For selected examples of helical “figure eight” macrocycles see: (a)Shimizu S, Cho W-S, Sessler JL, Shinokubo H, Osuka A. Chem. Eur. J 2008;14:2668–2678.2678 (b)Karle IL, Venkateshwarlu P, Nagaraj R, Sarma AVS, Vijay D, Sastry NG, Ranganathan S. Chem. Eur. J 2007;13:4253–4263.4263 (c)Katayev EA, Pantos GD, Reshetova MD, Khrustalev VN, Lynch VM, Ustynuk YA, Sessler JL. Angew. Chem. Int. Ed 2005;44:7386–7390.7390 (d)Werner A, Michels M, Zander L, Lex J, Vogel E. Angew. Chem. Int. Ed 1999;38:3650–3653.3653 (e)Sessler JL, Weghorn SJ, Lynch V, Johnson M-R. Angew. Chem. Int. Ed 1994;33:1509–1512.1512
2. Gregoliński J, Lisowski J. Angew. Chem. Int. Ed 2006;45:6122–6126.
3. (a) Gregoliński J, Ślepokura K, Lisowski J. Inorg. Chem 2007;46:7923–7934. [PubMed: 17705368] (b) Radecka-Paryzek W, Patroniak V, Lisowski J. Coord. Chem. Rev 2005;249:2156–2175. (c) Lisowski J, Ripoli S, Di Bari L. Inorg. Chem 2004;43:1388–1394. [PubMed: 14966974] (d) Lisowski J, Starynowicz P. Inorg. Chem. Comm 2003;6:593–597. (e) Lisowski J, Mazurek J. Polyhedron 2002;21:811–816. (f) Bligh SWA, Choi N, Evagorou EG, McPartlin M, White KN. J. Chem. Soc. Dalton Trans 2001:3169–3172. (g) Lisowski J, Starynowicz P. Polyhedron 1999;18:443–450. (h) Lisowski J, Starynowicz P. Polyhedron 2000;19:465–469. (i) Bligh SWA, Choi N, Evagorou EG, Li W-S, McPartlin M. Chem. Commun 1994:2399–2400.
4. For selected examples of helical macrocyclic complexes, see: (a)Hutin M, Schalley CA, Bernardinelli G, Nitschke JR. Chem. Eur. J 2006;12:4069–4076.4076 (b)Houjou H, Iwasaki A, Ogihara T, Kanesato M, Akabori S, Hiratani K. New J. Chem 2003;27:886–889.889 (c)Meskers SCJ, Dekkers HPJM, Rapanne G, Sauvage J-P. Chem. Eur. J 2000;6:2129–2134.2134 (d)Comba P, Fath A, Hambley TW, Kühner A, Richens DT, Vielfort A. Inorg. Chem 1998;37:4389–4401.4401 [PubMed: 11670576] (e) Fenton DE, Matthews RW, McPartlin M, Murphy BP, Scowen IJ, Tasker PA. J. Chem. Soc., Chem. Commun 1994:1391–1392.1392 (f)Matthews RW, McPartlin M, Scowen IJ. Chem. Commun 1996:309–310.310
5. Paluch M, Lisowski J, Lis T. Dalton Trans 2006:381. [PubMed: 16365653]
6. For selected recent examples of helical metallamacrocyclic complexes, see: (a)Li G, Yu W, Cui Y. J. Am. Chem. Soc 2008;130:4582–4583.4583 [PubMed: 18345674] (b)Li G, Yu W, Ni J, Liu T, Liu Y, Sheng E, Cui Y. Angew. Chem. Int. Ed 2008;47:1245–1249.1249 (c)Fukuda M, Sekiya R, Kuroda R. Angew. Chem. Int. Ed 2008;47:706–710.710 (d)Heo J, Jeon Y-M, Mirkin CA. J. Am. Chem. Soc 2007;129:7712–7713.7713 [PubMed: 17539639] (e)Funeriu DP, Rissanen K, Lehn J-M. Proc. Natl. Acad. Sci. USA 2001;98:10546–10551.10551 [PubMed: 11535827]
7. (a) Knof U, von Zelewsky A. Angew. Chem. Int. Ed 1999;38:302–322. (b) Mateos-Timoneda MA, Crego-Calama M, Reinhoudt DN. Chem. Soc. Rev 2004;33:363–372. [PubMed: 15280969] (c) Cornelissen JJLM, Rowan AE, Nolte RJM, Sommerdiijk NAJM. Chem. Rev 2001;101:4039–4070. [PubMed: 11740926]
8. For selected examples see: (a)Xu J, Raymond KN. Angew. Chem. Int. Ed 2006;45:6480–6485.6485 (b)Yeh RM, Raymond KN. Inorg. Chem 2006;45:1130–1139.1139 [PubMed: 16441123] (c)Zeckert K, Hamacek J, Senegas J-M, Dalla-Favera N, Floquet S, Bernardinelli G, Piguet C. Angew. Chem. Int. Ed 2005;44:7954–7958.7958 (d)Baylies CJ, Riis-Johannessen T, Harding LP, Jeffery JC, Moon R, Rice CR, Whitehead M. Angew. Chem. Int. Ed 2005;44:6909–6912.6912 (e)Bassett AP, Magennis SW, Glover PB, Lewis DJ, Spencer N, Parsons S, Williams RM, De Cola L, Pikramenou Z. J. Am. Chem. Soc 2004;126:9413–9424.9424 [PubMed: 15281834] (f)Cantuel M, Bernardinelli G, Muller G, Riehl JP, Piguet C. Inorg. Chem 2004;43:1840–1849.1849 [PubMed: 15018502] (g)Bowyer PK, Cook VC, Gharib-Naseri N, Gugger PA, Rae AD, Swiegers GF, Willis AC, Zank J, Wild SB. Proc. Natl. Acad. Sci. USA 2002;99:4877–4882.4882 [PubMed: 11929976] (h)Hasenknopf B, Lehn J-M, Boumediene N, Leize E, Van Dorsselaer A. Angew. Chem. Int. Ed 1998;37:3265–3268.3268 (i) Albrecht M. Chem. Rev 2001;101:3457–3497.3497 [PubMed: 11840991] (j)Piguet C, Bernardinelli

G, Hopfgartner G. Chem. Rev 1997;97:2005–2062.2062 [PubMed: 11848897] (k)Woods CR, Benaglia M, Siegel JS, Cozzi F. Angew. Chem. Int. Ed 1996;35:1830–1833.1833

9. (a) Parker D. Chem. Soc. Rev 2004;33:156–165. [PubMed: 15026820] (b) Di Bari L, Pescitelli G, Sherry AD, Woods M. Inorg. Chem 2005;44:8391–8398. [PubMed: 16270977] (c) Woods M, Kovacs Z, Zhang S, Sherry AD. Angew. Chem. Int. Ed 2003;42:5889–5892. (d) Dickins RS, Howard JAK, Lehmann CW, Moloney J, Parker D, Peacock RD. Angew. Chem. Int. Ed 1997;36:521–523. (e) Dickins RS, Aime S, Batsanov AS, Beeby A, Botta M, Bruce JI, Howard JAK, Love CS, Parker D, Peacock RD, Puschmann H. J. Am. Chem. Soc 2002;124:12697–12705. [PubMed: 12392417]
10. For examples of diastereoselective formation of lanthanide helical complexes see: (a)Petoud S, Muller G, Moore EG, Xu J, Sokolnicki J, Riehl JP, Le UN, Cohen SM, Raymond KN. J. Am. Chem. Soc 2007;129:77–83.83 [PubMed: 17199285] (b)Leonard JP, Jensen P, McCabe T, O'Brien JE, Peacock RD, Kruger PE, Gunnlaugsson T. J. Am. Chem. Soc 2007;129:10986–10987.10987 [PubMed: 17696537] (c)Lama M, Mamula O, Kottas GS, Rizzo F, De Cola L, Nakamura A, Kuroda R, Stoeckli-Evans H. Chem. Eur. J 2007;13:7358–7373.7373 (d)Albrecht M, Schimid S, Dehn S, Wickleder C, Zhang S, Basset AP, Pikramenou Z, Fröhlich R. New J. Chem 2007;31:1755–1762.1762 (e)Jeong KS, Kim YS, Kim YJ, Lee E, Yoon JH, Park WH, Park YW, Jeon S-J, Kim ZH, Kim J, Jeong N. Angew. Chem. Int. Ed 2006;45:8134–8138.8138 (f)Mamula O, Lama M, Telfer SG, Nakamura A, Kuroda R, Stoeckli-Evans H, Scopelitti R. Angew. Chem. Int. Ed 2005;44:2527–2531.2531
11. For controlled helicity inversion in inorganic systems see: (a)Miyake H, Hikita M, Itazaki M, Nakazawa H, Sugimoto H, Tsukube H. Chem. Eur. J 2008;14:5393–5396.5396 (b)Miyake H, Kamon H, Miyahara I, Sugimoto H, Tsukube H. J. Am. Chem. Soc 2008;130:792–793.793 [PubMed: 18161973] (c)Miyake H, Sugimoto H, Tamiaki H, Tsukube H. Chem. Commun 2005:4291–4293.4293 (d)Miyake H, Yoshida K, Sugimoto H, Tsukube H. J. Am. Chem. Soc 2004;126:6524–6525.6525 [PubMed: 15161259] (e)Hutin M, Nitschke J. Chem. Commun 2006:1724–1726.1726 (f) Zahn S, Canary JW. Science 2000;288:1404–1407.1407 [PubMed: 10827947] (g)Zahn S, Das D, Canary JW. Inorg. Chem 2006;45:6056–6063.6063 [PubMed: 16842014] (h)Biscarini P, Kuroda R. Inorg. Chim. Acta 1988;154:209–214.214
12. For examples of controlled helicity inversion in organic polymeric systems see: (a)Okoshi K, Sakurai S-i, Ohsawa S, Kumaki J, Yashima E. Angew. Chem. Int. Ed 2006;45:8173–8176.8176 (b)Sakurai, S-i; Okoshi, K.; Kumaki, J.; Yashima, E. J. Am. Chem. Soc 2006;128:5650–5651.5651 [PubMed: 16637628] (c)Maeda K, Mochizuki H, Watanabe M, Yashima E. J. Am. Chem. Soc 2006;128:7639–7650.7650 [PubMed: 16756321] (d)Tang H-Z, Novak BM, He J, Polavarapu PL. Angew. Chem. Int. Ed 2005;44:7298–7301.7301 (e)Tang H-Z, Boyle PD, Novak BM. J. Am. Chem. Soc 2005;127:2136–2142.2142 [PubMed: 15713090] (f)Tang K, Green MM, Cheon KS, Selinger JV, Garetz BA. J. Am. Chem. Soc 2003;125:7313–7323.7323 [PubMed: 12797806]
13. (a) Meudtner RM, Hecht S. Angew. Chem. Int. Ed 2008;47:4926–4930. (b) Hembury GA, Borovkov VV, Inoue Y. Chem. Rev 2008;108:1–73. [PubMed: 18095713] (c) Hofacker AL, Parquette JR. Angew. Chem. Int. Ed 2005;44:1053–1057. (d) Borovkov VV, Hembury GA, Inoue Y. Angew. Chem. Int. Ed 2003;42:5310–5314.
14. For examples of controlled helicity inversion in supramolecular polymeric aggregates see: (a)Johnson RS, Yamazaki T, Kovalenko A, Fenniri H. J. Am. Chem. Soc 2007;129:5735–5743.5743 [PubMed: 17417852] (b)Ajayaghosh A, Varghese R, George SJ, Vijayakumar C. Angew. Chem. Int. Ed 2006;45:1141–1144.1144 (c)Lohr A, Lysetska M, Würthner F. Angew. Chem. Int. Ed 2005;44:5071–5074.5074
15. (a) Pijper D, Jongejan MGM, Meetsma A, Feringa BL. J. Am. Chem. Soc 2008;130:4541–4552. [PubMed: 18335940] (b) Vicario J, Katsonis N, Serrano Ramon B, Bastiaansen CWM, Broer DJ, Feringa BL. Nature 2006;440 (c) ter Viel MKJ, Van Delden RA, Meetsma A, Feringa BL. J. Am. Chem. Soc 2003;125:15076–15086. [PubMed: 14653742]
16. Belmont P, Constant J-F, Demeunynck M. Chem. Soc. Rev 2001;30:70–81.
17. (a) Gonzalez-Alvarez A, Alfonso I, Lopez-Oritz F, Aguirre A, Garcia-Granda S, Gotor V. Eur. J. Org. Chem 2004:1117–1127. (b) Kuhnert N, Rossignolo GM, Lopez-Periago A. Org. Biomol. Chem 2003;1:1157–1170. [PubMed: 12926390]
18. As a consequence of the Cahn-Ingold-Prelog sequence rules, the *R* configuration at coordinated nitrogen atom corresponds to the *S* configuration of the respective form of the free macrocycle **L**.

19. Tancrez N, Feuvrie C, Ledoux I, Zyss J, Toupet L, Le Bozec H, Maury O. J. Am. Chem. Soc 2005;127:13474–13475. [PubMed: 16190692]
20. Lisowski J, Sessler JL, Lynch V, Mody TD. J. Am. Chem. Soc 1995;117:2273–2285.
21. (a) Du W, Xia Z, Dewilde S, Moens L, La Mar GN. Eur. J. Biochem 2003;270:2707–2720. [PubMed: 12823541](b)LecomteJTJLa MarGNJ. Am. Chem. Soc198710972197220; (c) Thanabal V, de Ropp JS, La Mar GN. J. Am. Chem. Soc 1988;110:3027–3035.
22. Medforth CJ, Shiau F-Y, La Mar GN, Smith KM. J. Chem. Soc., Chem. Commun 1991:590–592.
23. Marzilli LG, Polson SM, Hansen L, Moore SJ, Marzilli PA. Inorg. Chem 1997;36:3854–3860.
24. Steemers FJ, Verboom W, Reinhoudt DN, van der Tol EB, Verhoeven JW. J. Am. Chem. Soc 1995;117:9488–9414.
25. Beeby A, Clarkson IM, Dickins RS, Faulkner S, Parker D, Royle L, de Sousa AS, Williams JAG, Woods M. J. Chem. Soc., Perkin Trans 1999;2:493–504.
26. Supkowski RM, Horrocks WDeW. Inorg. Chim. Acta 2002;340:44–48.
27. Wang Z, Choppin GR, Di Bernardo P, Zanonato P-L, Portanova R, Tolazzi M. J. Chem. Soc. Dalton Trans 1993:2791–2796.
28. Riehl, JP.; Muller, G. Handbook on the Physics and Chemistry of Rare Earths. Gschneidner, KA.; Bunzli, J-CG.; Pecharsky, VK., editors. Vol. Vol. 34. Amsterdam: North-Holland Publishing; 2005. (b) Do K, Muller FC, Muller G. J. Phys. Chem. A 2008;112:6789–6793. [PubMed: 18597442] (c) Lunkley JL, Shirotani D, Yamanari K, Kaizaki S, Muller G. J. Am. Chem. Soc 2008;130:13814–13815. [PubMed: 18816117]
29. For selected recent examples of Ln(III)-based CPL studies, see: (a)Seitz M, Moore EG, Ingram AJ, Muller G, Raymond KN. J. Am. Chem. Soc 2007;129:15468–15470.15470 [PubMed: 18031042] (b) Bonsall SD, Houcheime M, Straus DA, Muller G. Chem. Commun 2007:3676–3678.3678 (c) Leonard JP, Jensen P, McCabe T, O'Brien JE, Peacock RD, Kruger PE, Gunnlaugsson T. J. Am. Chem. Soc 2007;129:10986–10987.10987 [PubMed: 17696537] (d)Pedziwiatr M, Kosareff NM, Muller G, Koposov AY, Nemykin VN, Riehl JP, Legendziewicz J. J. Alloys Compnds 2008;451:251–253.253 (e)Montgomery CP, New EJ, Parker D, Peacock RD. Chem. Commun 2008:4261–4263.4263
30. Meech SR, Phillips DC. J. Photochem 1983;23:193–217.
31. Chauvin A-S, Gumy F, Imbert D, Bünzli J-CG. Spectroscopy Lett 2004;37:517–532.
32. ver. 1.171 Oxford Diffraction Poland. 1995–2003. KM4CCD software: CRYSALIS CCD and CRYSALIS RED.
33. Sheldrick, GM. Program for the Solution of Crystal Structures. Göttingen (Germany): University of Göttingen; 1997. SHELXS-97.
34. Sheldrick, GM. Program for the Refinement of Crystal Structures. Göttingen (Germany): University of Göttingen; 1997. SHELXL-97.
35. Sheldrick, GM. Version 6.10. Madison, WI, USA: Bruker AXS; 2000. SHELXTL.
36. Ver. 1.4.1, Program for Crystal Structure Visualization and Exploration. CCDC Cambridge University; MERCURY.
37. Brandenburg, K. DIAMOND Crystal Imact GbR. Germany: Bonn; 2006.

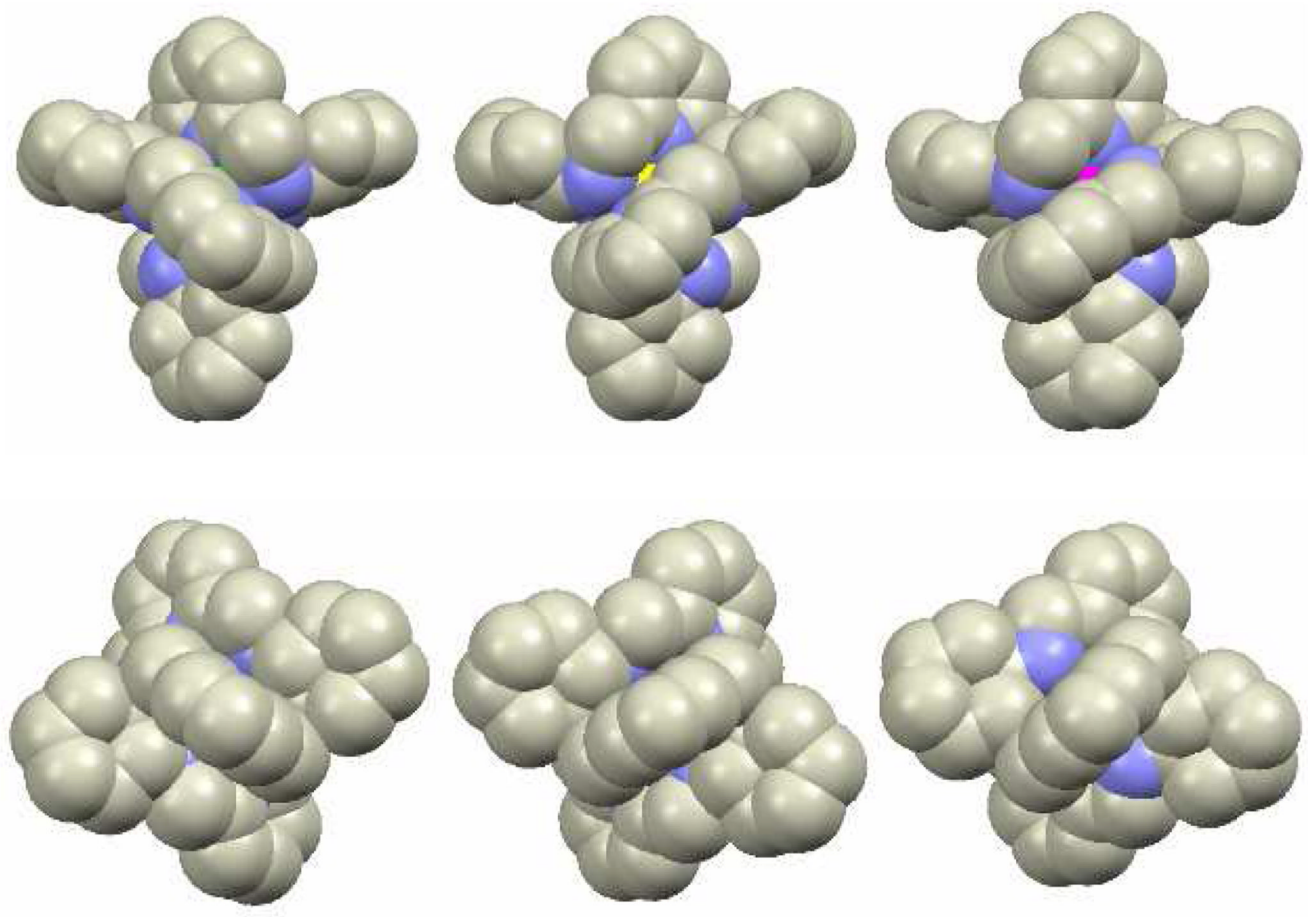

**Fig. 1.**
Top: views along the direction perpendicular to the $C_2$ axis of the structures of the *(M)*-[Pr**L**$_{RRRRRR}$]$^{3+}$ (right), *(P)*-[Ce**L**$_{SSSSSS}$]$^{3+}$ (middle) and *(P)*-[Lu**L**$_{RRRRRR}$]$^{3+}$ (right) macrocyclic complexes. Bottom: views along the $C_2$ axis of the same complexes.

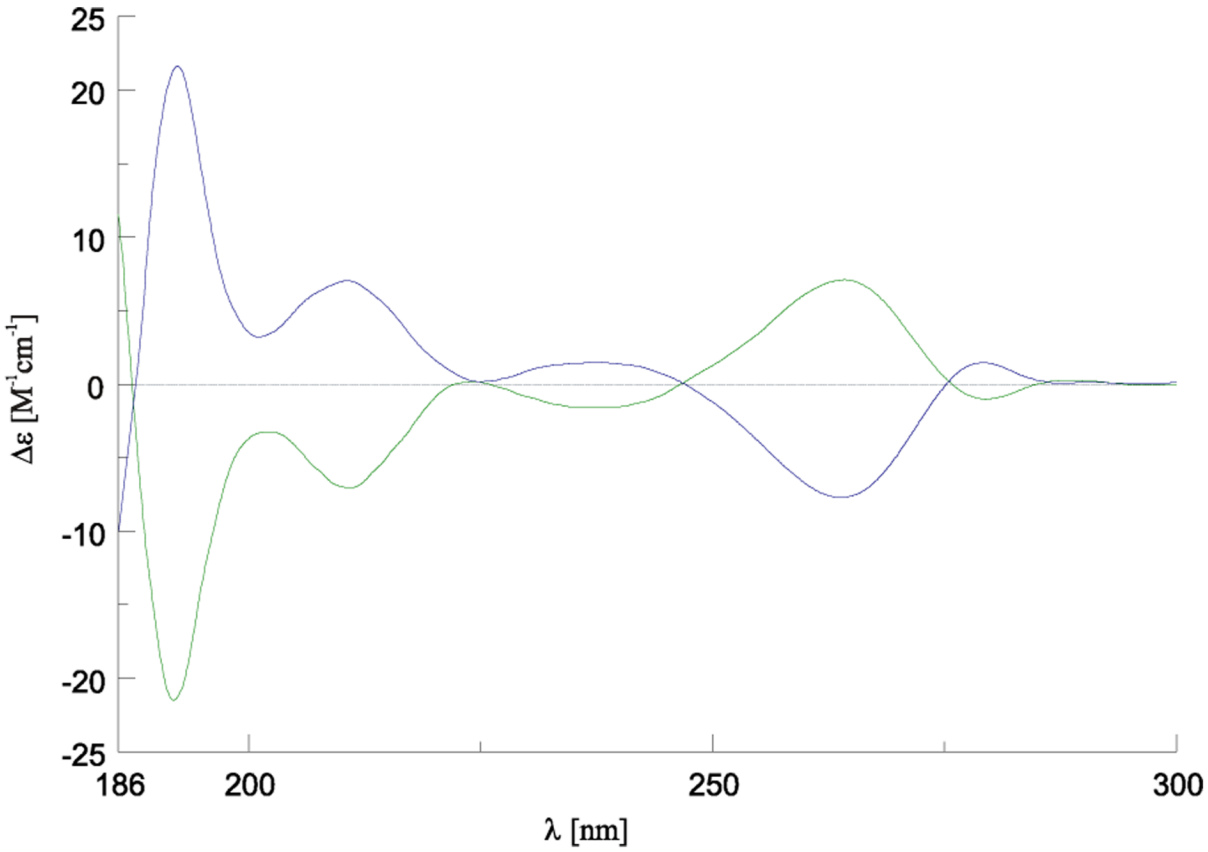


**Fig. 2.**

The CD spectra of the two enantiomeric [Nd**L**]$(NO_3)_3$•0.5$H_2O$ complexes in 1 × $10^{-3}$ M $H_2O$ solutions: (*M*)-[Nd$\mathbf{L}_{RRRRRR}$]$^{3+}$ (green ) and (*P*)-[Nd$\mathbf{L}_{SSSSSS}$]$^{3+}$ (blue).

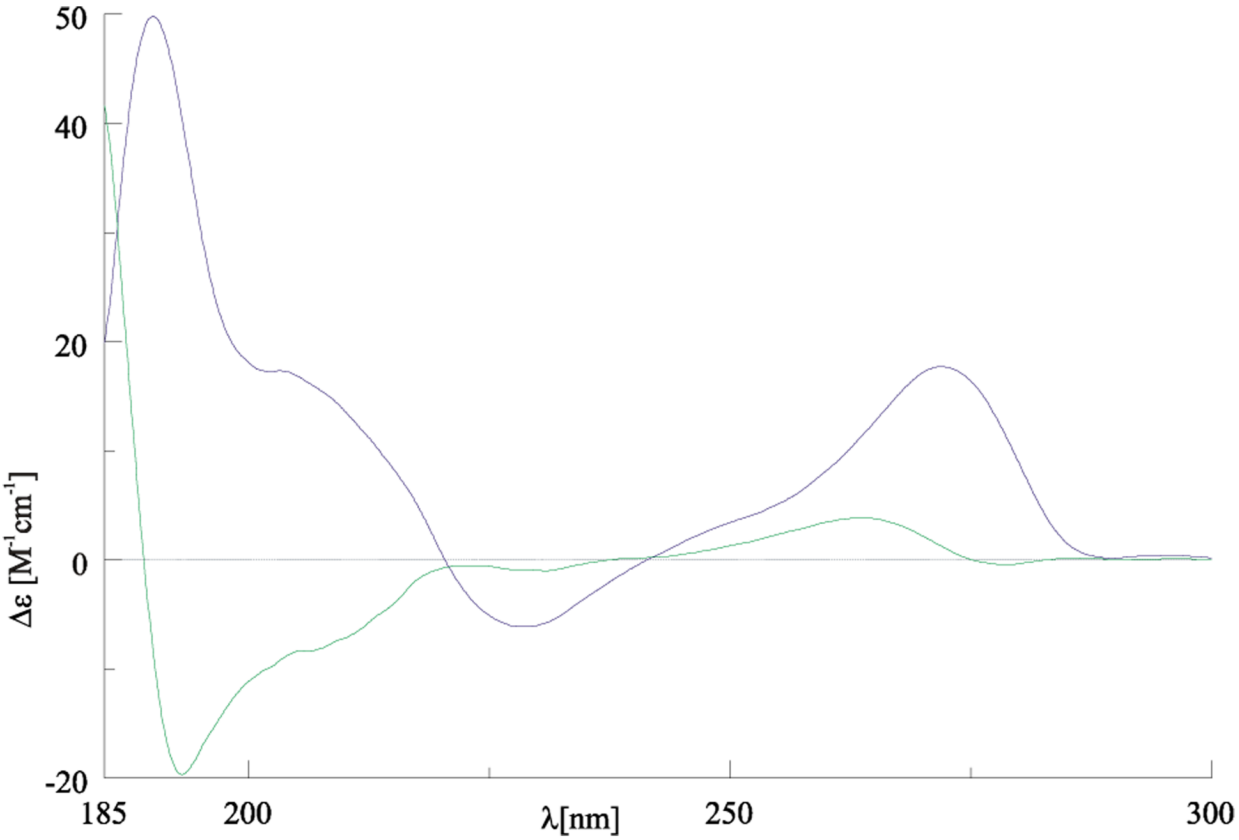


**Fig. 3.**
The CD spectra of the two diastereomers of the Er(III) complexes with $\mathbf{L}_{RRRRRR}$ in $1 \times 10^{-3}$ M $H_2O$ solutions: (*M*)-[Er$\mathbf{L}_{RRRRRR}$]$^{3+}$ (green) and (*P*)-[Er$\mathbf{L}_{RRRRRR}$]$^{3+}$ (blue).

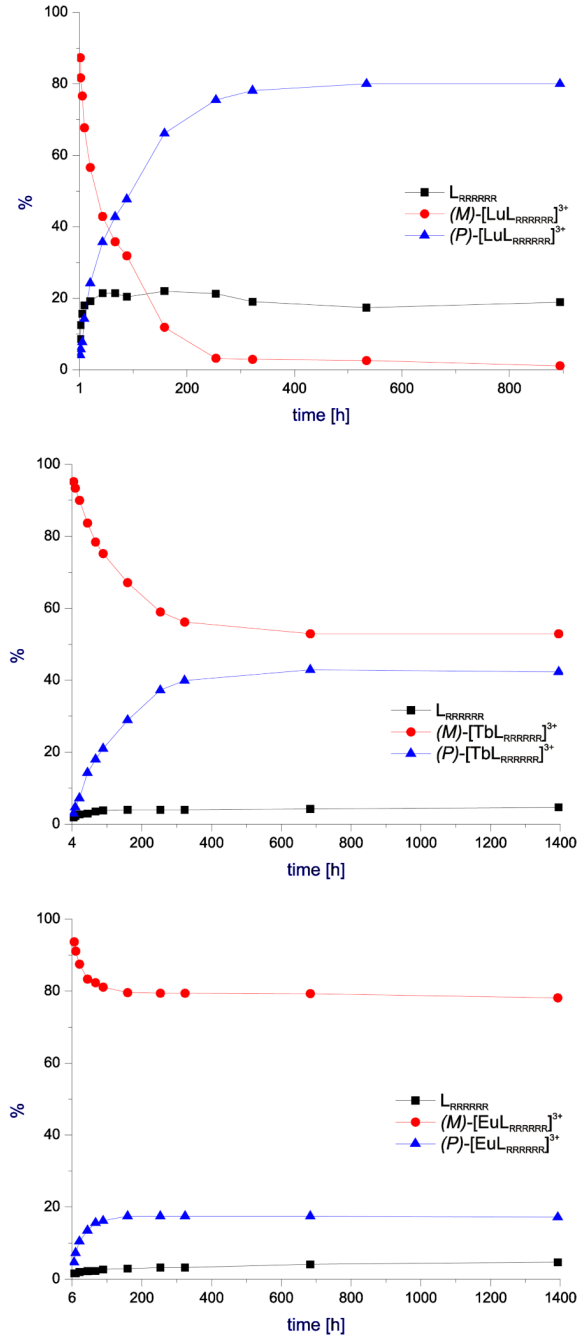


**Fig. 4.**

The dependence of the relative concentration of the (*M*)- and (*P*)-diastereomers on the heating time of $1 \times 10^{-2}$ M solutions of (*M*)-[Ln$\mathbf{L}_{\boldsymbol{RRRRRR}}$]$(NO_3)_3$ complexes ($D_2O$, 318K). The red, blue and black plots represent the (*M*)- and (*P*)-[Ln$\mathbf{L}_{\boldsymbol{RRRRRR}}]^{3+}$ complexes, and the free ligand $\mathbf{L}_{\boldsymbol{RRRRRR}}$, respectively.

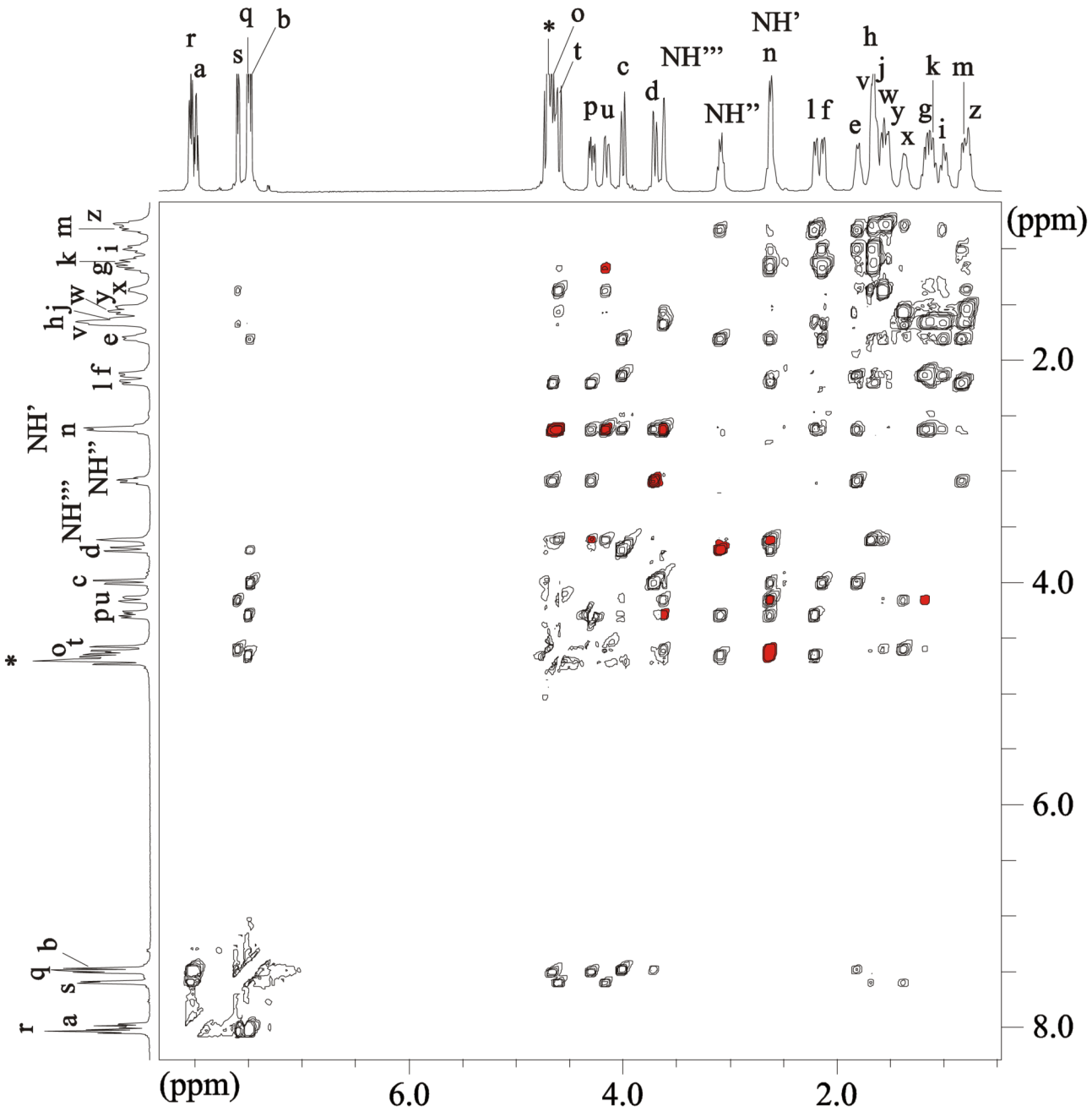


**Fig. 5.**

The ROESY spectrum of the (*P*)-[Lu**L**$_{RRRRRR}$](NO$_3$)$_3$•7H$_2$O complex (D$_2$O, 298K). Red color indicates the cross-peaks corresponding to short distances characteristic for the twisted form of the macrocycle (see text for details).

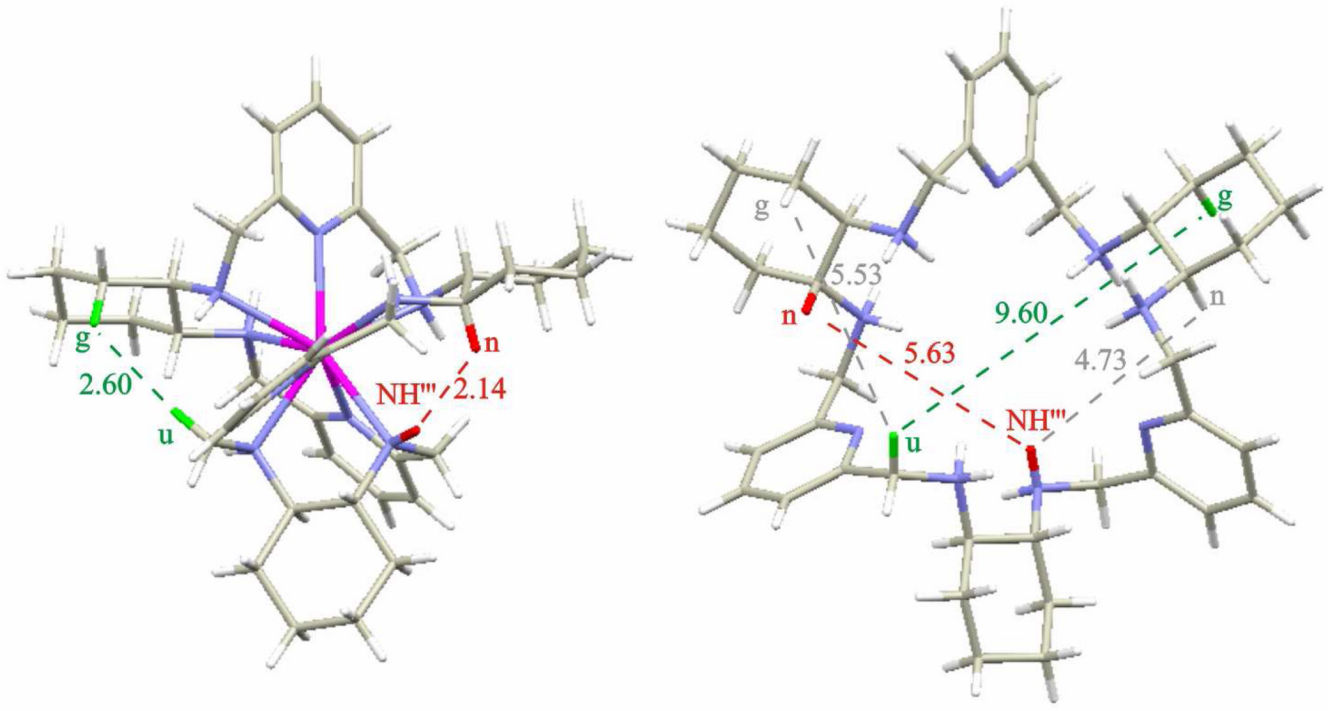


**Fig. 6.**

The comparison of the inter-proton distances between the structures of *(P)*-[Lu**L**$_{RRRRRR}$]$^{3+}$ complex (left) and the protonated free macrocycle (right). The two indicated coloured distances correspond to the same pairs of protons **u-g** (green) and **NH'''-n** (red).

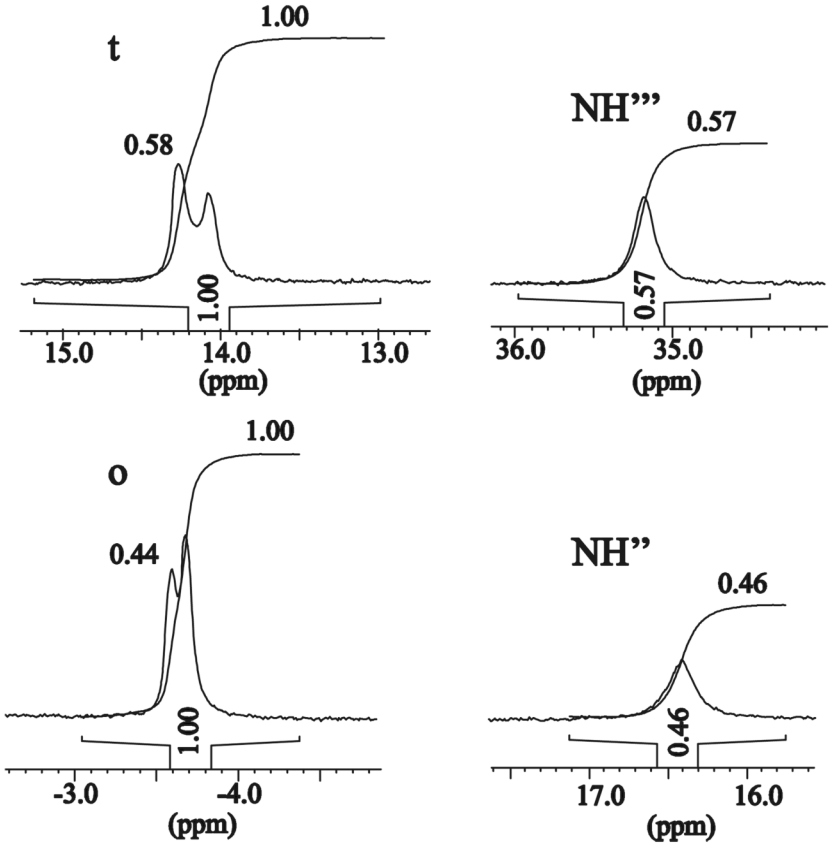


**Fig. 7.**

The fragments of the $^{1}$H NMR spectrum (298K, $CD_3OD/CDCl_3$ 1:2 v/v) of the partially deuterated (*M*)-[Eu**L**$_{RRRRRR}$]$(NO_3)_3$•$4H_2O$ complex illustrating the doubling of the signals **o** and **t**, correlated to the changes of intensity of signals **NH"** and **NH'"**, respectively.

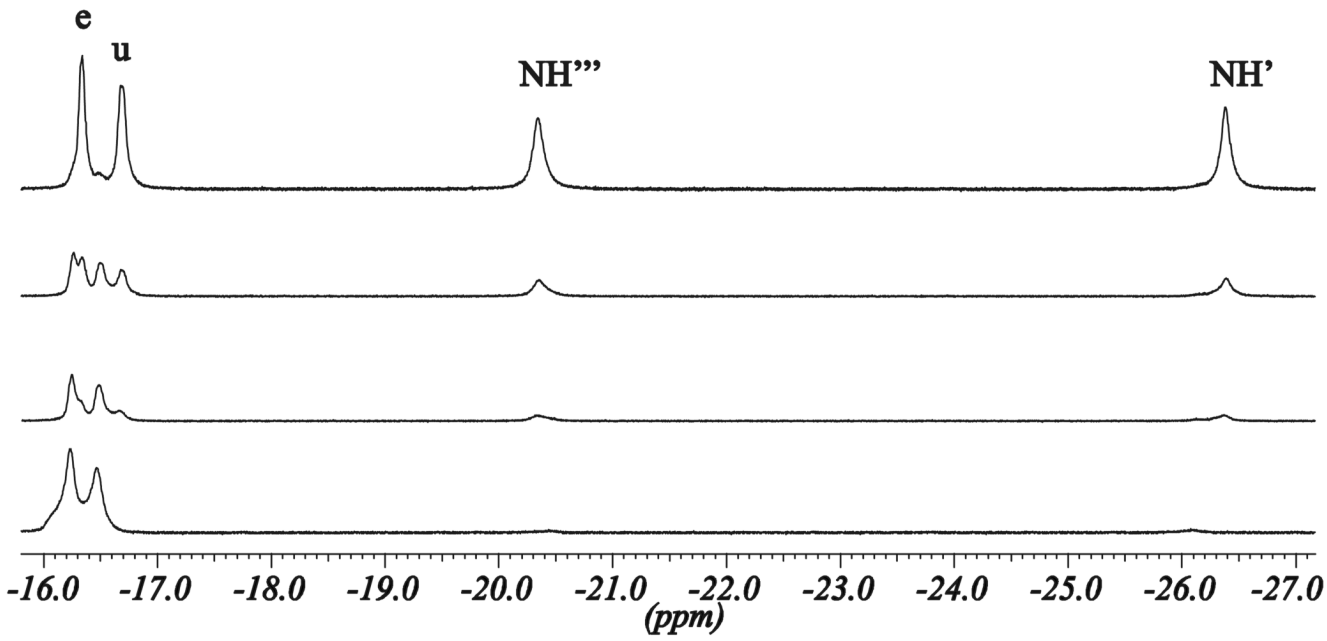


**Fig. 8.**

The fragments of the $^{1}$H NMR spectra recorded over 27 h (298K, $CD_3OD/CD_3CN$) of the *(M)*-[Pr**L**$_{RRRRRR}$]$(NO_3)_3 \cdot H_2O$ complex, illustrating the doubling of the resonances due to isotope effect. Spectra measured after (from top) 15 min, 2 h 30 min, 5 h and 27 h.

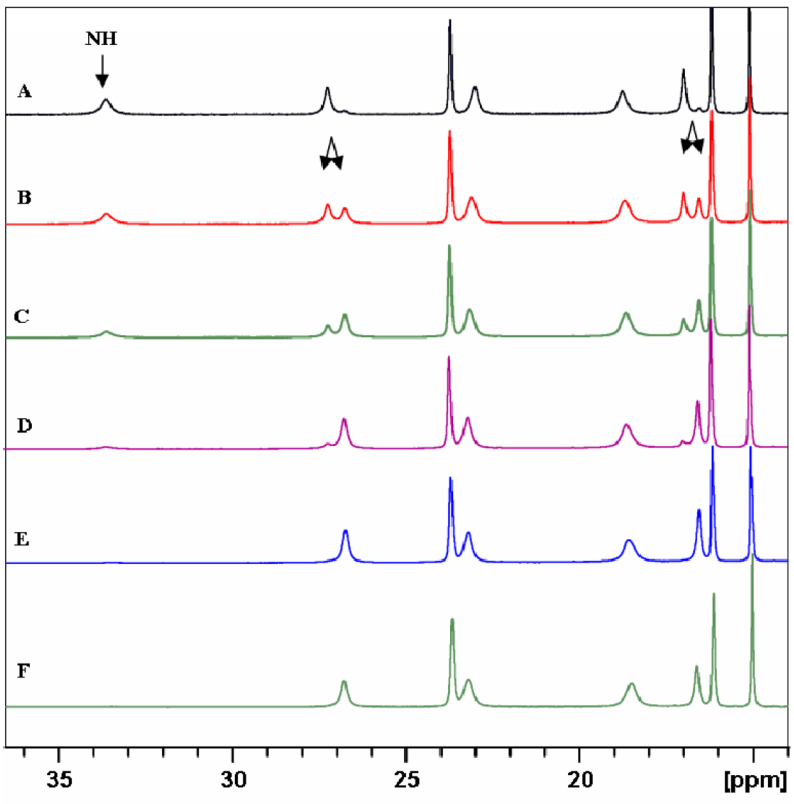


**Fig. 9.**

The fragments of the $^{1}$H NMR spectra (298K, $CD_3OD$) of (*P*)-[Yb**L**$_{RRRRRR}$]$(NO_3)_3$•$6H_2O$ complex, illustrating the disappearing of NH signal, doubling of the resonances due to isotope effect and the influence of added base. Traces A – E : spectra measured after 0.45 h, 1.45 h, 2.45 h, 4.45h, and 27h, respectively; trace F: spectrum of a sample containing 5 μL of N$(C_2H_5)_3$ measured after 0.25 h.

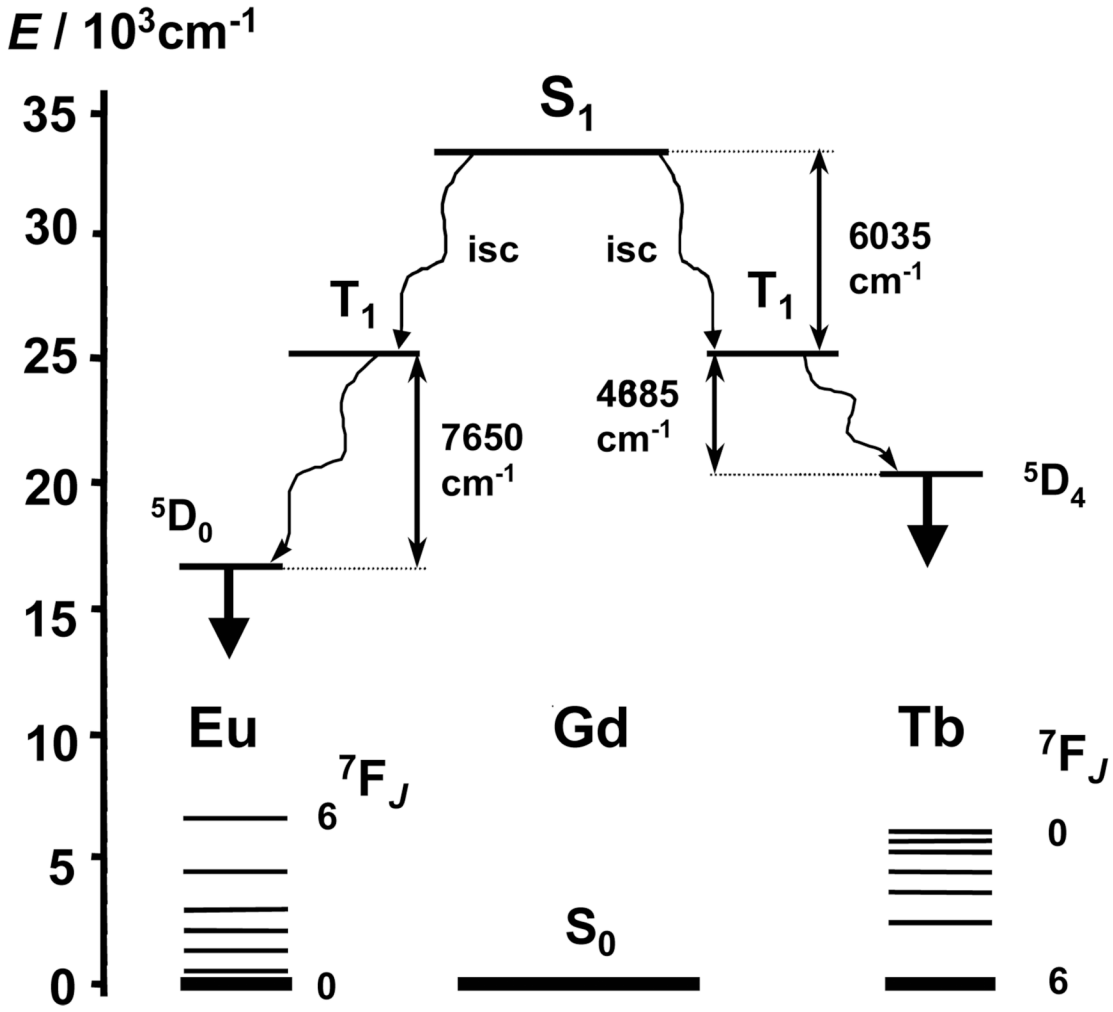


**Figure 10.**
Schematic energy diagram for Eu(III)- and Tb(III)-containing complexes with $\mathbf{L}_{RRRRRR}$. Data for $S_1$ and $T_1$ are those of the Gd(III) complex in frozen MeOH solution at 77 K.

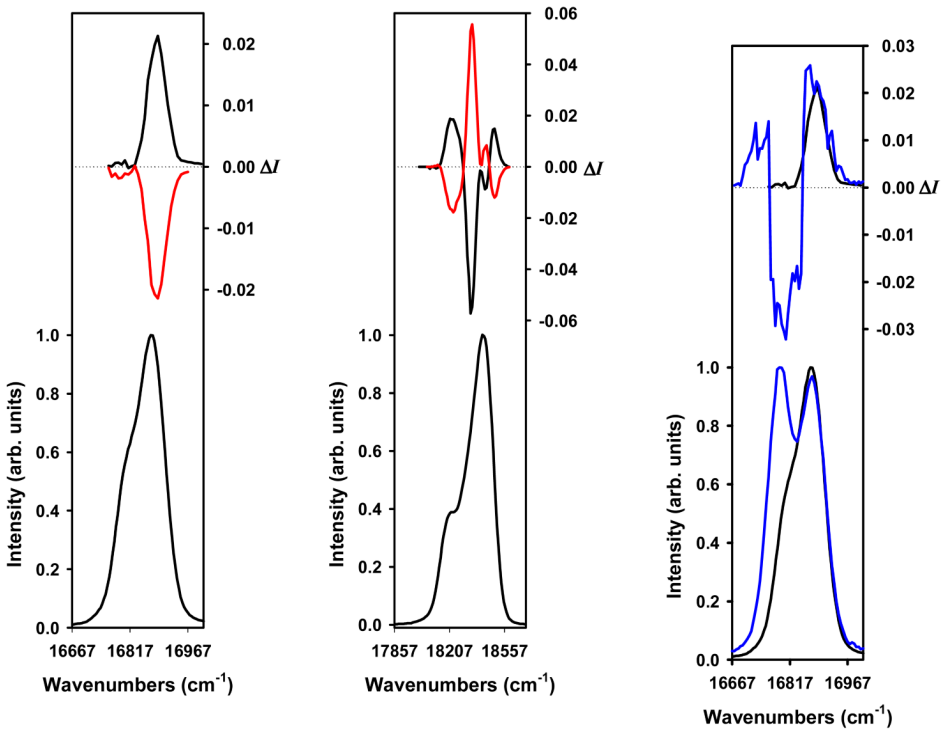


**Figure 11.**

Circularly polarized luminescence (upper curve) and total luminescence (lower curve) spectra of (*M*)-[Ln$\mathbf{L}_{RRRRRR}$]$^{3+}$ (Ln = Eu, Tb, black) and (*P*)-[Ln$\mathbf{L}_{SSSSSS}$]$^{3+}$ (Ln = Eu, Tb, red) in 1 × $10^{-2}$ M MeOH at 295 K, upon excitation at 283–284 nm, respectively. Left: $^5D_0 \rightarrow {}^7F_1$ (Eu) transition, middle: $^5D_4 \rightarrow {}^7F_5$ (Tb) transition, and right: $^5D_0 \rightarrow {}^7F_1$ transition of (*M*)-[Eu$\mathbf{L}_{RRRRRR}$]$^{3+}$ (black) and a 3.5:1 (*M*)-[Eu$\mathbf{L}_{RRRRRR}$]$^{3+}$:(*P*)-[Eu$\mathbf{L}_{RRRRRR}$]$^{3+}$ complex solution (blue).

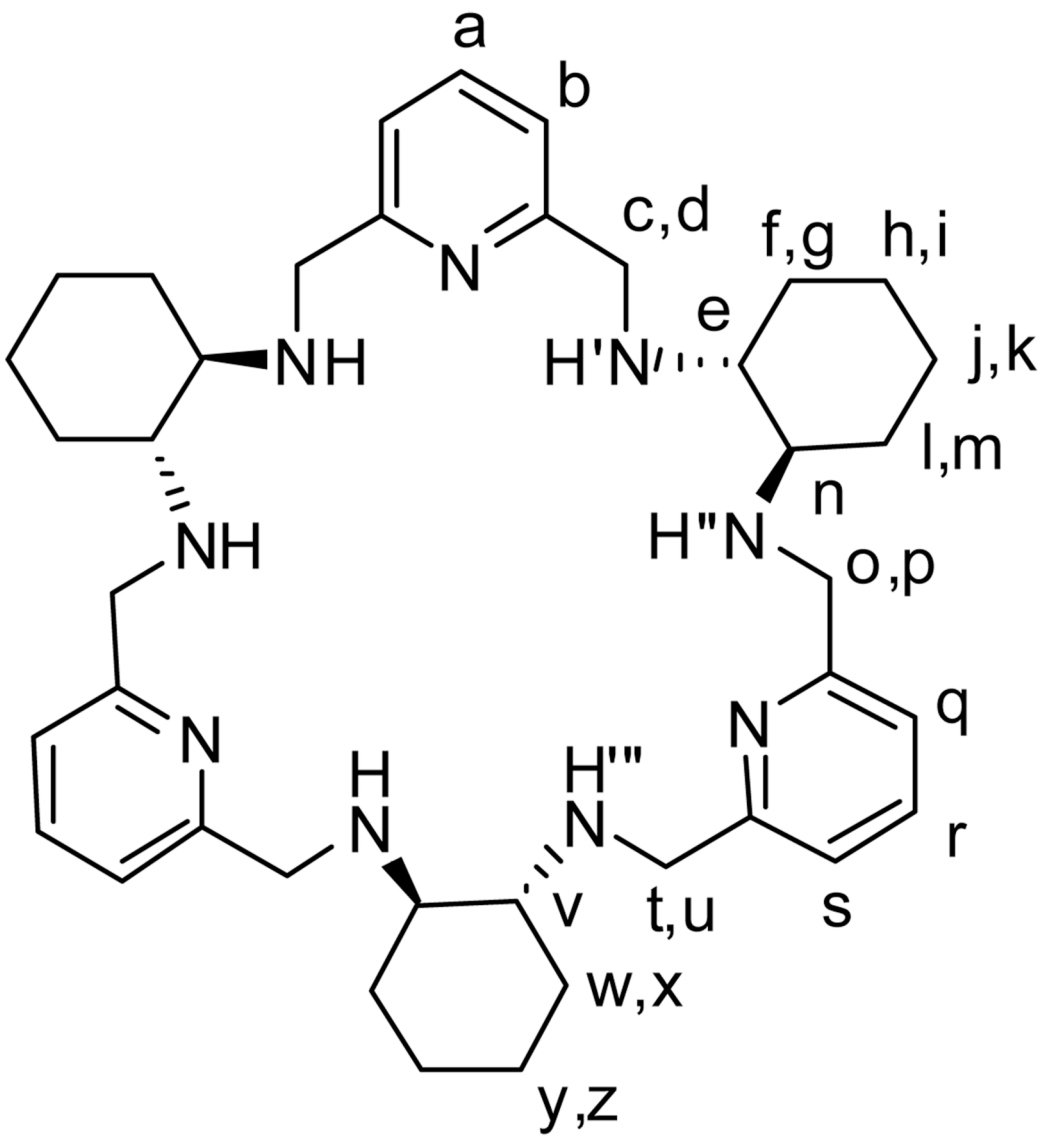


**Scheme 1.**
The macrocycle $\mathbf{L}_{RRRRRR}$ and its labeling scheme

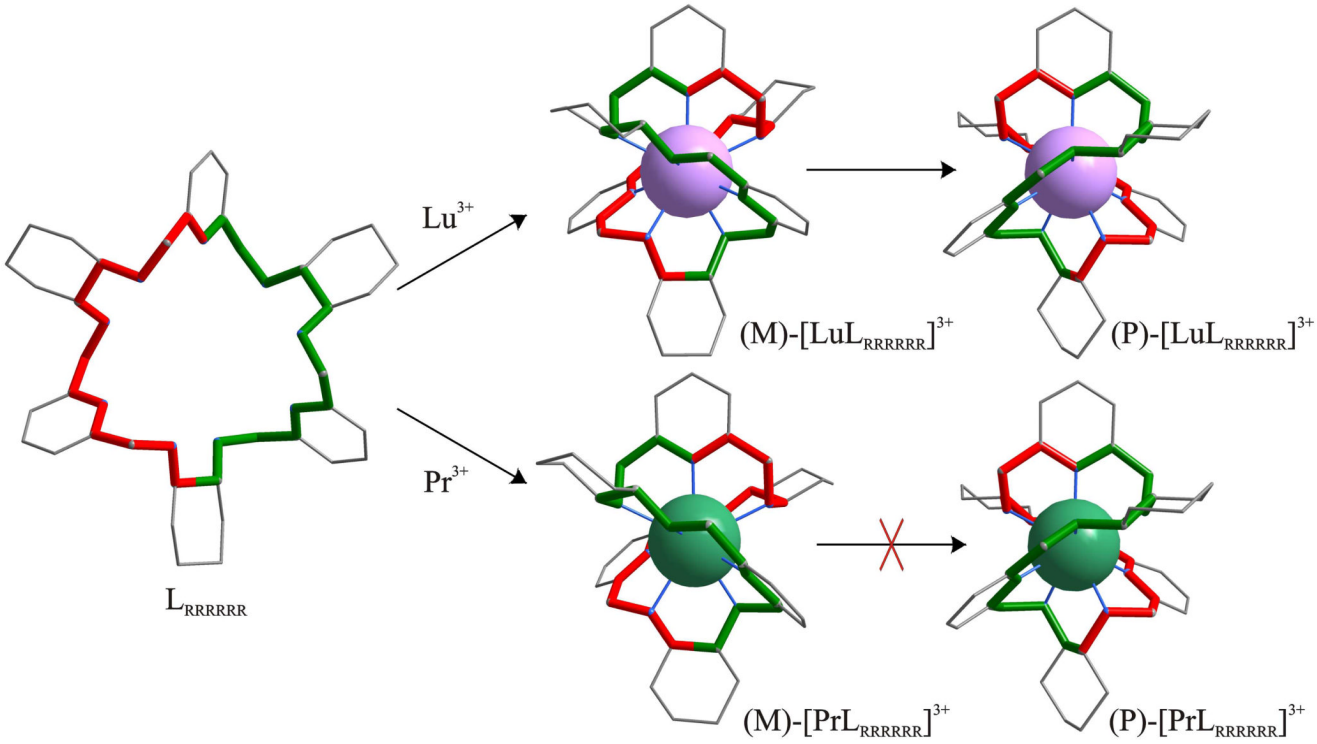


**Scheme 2.**

Formation, helicity inversion and X-ray crystal structures of the $[Ln\mathbf{L}]^{3+}$ complexes. The structures of (*M*)-$[Pr\mathbf{L}_{\boldsymbol{RRRRRR}}]^{3+}$ and (*P*)-$[Lu\mathbf{L}_{\boldsymbol{RRRRRR}}]^{3+}$ complex cations are based on crystallographic data reported in this work, the drawing of the macrocyle $\mathbf{L}_{\boldsymbol{RRRRRR}}$ is based on the crystallographic data of the protonated ligand[17a] and the drawing of (*M*)-$[Lu\mathbf{L}_{\boldsymbol{RRRRRR}}]^{3+}$ is based on the crystallographic data of the isomorphic Yb(III) complex[2].

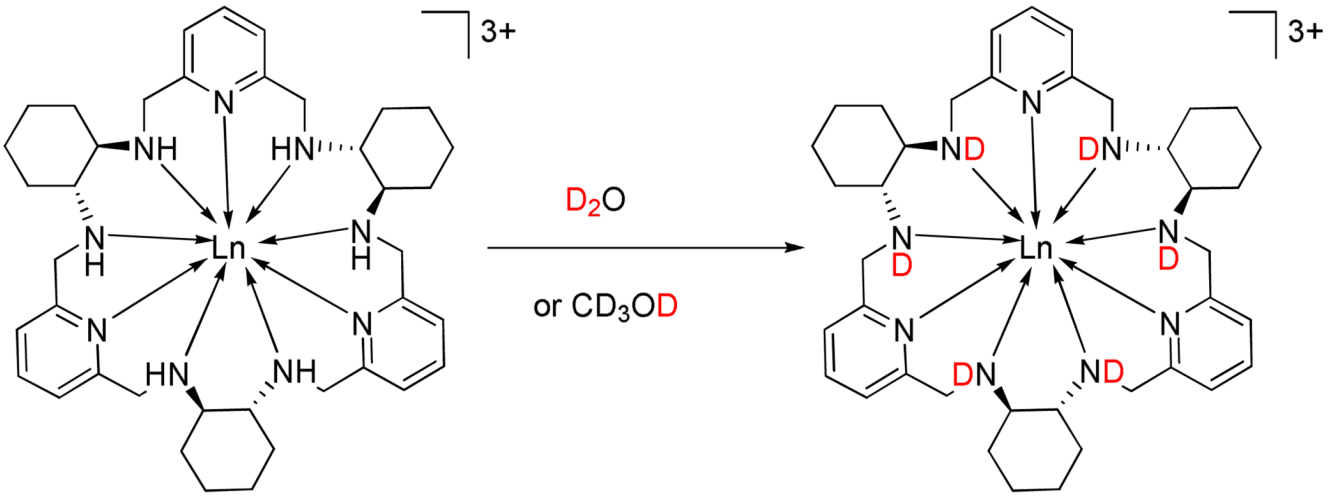


**Scheme 3.**
The NH/ND exchange in the [Ln**L**]$^{3+}$ complexes.

**Table 1**

Ligand-centred absorptions in MeOH solutions (295 K), ligand-centred singlet- and triplet-state energies as determined from emission spectra of solutions 2–3 × $10^{-5}$ and 3–4 × $10^{-4}$ M in MeOH (295 and 77 K) for the ligand $\mathbf{L}_{RRRRRR}$ and its Ln(III)-containing complexes, respectively.[a]

| Compound | $E(x\rightarrow\pi^*)/cm^{-1}$[b] solution[c] | $E(^1\pi\pi^*)/cm^{-1}$ solution | solid state[d] | $E(^3\pi\pi^*)/cm^{-1}$ solid state[d] |
|---|---|---|---|---|
| $\mathbf{L}_{RRRRRR}$ | 36 500 (4.10) sh | 33 615 | 29 585 (sh) | 24 905 |
| | 37 585 (4.22) | | 32 260 | |
| $[Gd\mathbf{L}_{RRRRRR}]^{3+}$ | 35 750 (4.40) sh | 32 305 | 30 910 (sh) | 24 875 |
| | 36 760 (4.57) | | 32 155 | 27 960 (sh) |
| $[Eu\mathbf{L}_{RRRRRR}]^{3+}$ | 35 750 (3.94) sh | 32 305 | *e* | *e* |
| | 36 770 (4.12) | | | |
| $[Tb\mathbf{L}_{RRRRRR}]^{3+}$ | 35 750 (4.00) sh | 32 305 | *e* | *e* |
| | 36 770 (4.18) | | | |

[a] sh = shoulder

[b] x = n or π

[c] At the concentration used, the $^1$H-NMR spectra recorded at room temperature and 213 K show only one set of signals suggesting the presence of only one diastereomer in MeOH solution; Logε values are given between parentheses

[d] Values given for frozen solutions in MeOH

[e] Not observed because of the $\mathbf{L}_{RRRRRR}$-to-Ln energy transfer process